13

Dye Solar Cells: Basic and Photon Management Strategies

Lorenzo Dominici[1,2] et al.[*]
[1]*Centre for Hybrid and Organic Solar Energy Centre (CHOSE), Dept. of Electronic Eng., Tor Vergata University of Rome, Roma*
[2]*Molecular Photonics Laboratory, Dept. of Basic and Applied Physics for Eng., SAPIENZA University of Rome, Roma*
Italy

1. Introduction

After the introduction in 1991 by B. O'Regan and M. Grätzel, Dye Solar Cells (DSCs) have reached power conversion efficiency values over small area device as high as 11%. Being manufactured with relatively easy fabrication processes often borrowed from the printing industry and utilizing low cost materials, DSC technology can be considered nowadays a proper candidate for a large scale production in industrial environment for commercial purposes.
This scenario passes through some challenging issues which need to be addressed such as the set-up of a reliable, highly automated and cost-effective production line and the increase of large area panels performances, in terms of efficiency, stability and life-time of the devices.
In this work, an overview of the most utilized DSCs materials and fabrication techniques are highlighted, and some of the most significant characterization methods are described. In this direction, different approaches used to improves devices performances are presented.
In particular, several methods and techniques known as Light Management (LM) have been reported, based to the ability of the light to be confined most of the time in the cell structure. This behavior contributes to stimulate higher levels of charge generation by exploiting scattering and reflection effects.
The use of diffusive scattering layers (SLs), nanovoids, photonic crystals (PCs), or photoanodes co-sensitization approaches consisting in the use of two Dyes absorbing in two different parts of the visible range, have been demonstrated to be effective strategies to carry out the highest values of device electrical parameters.
Finally, to increase the light path inside the DSCs active layer, the use of refractive element on the topside (a complementary approach to SL) has been shown a promising possibility to further improve the generated photocurrent.

[*]Daniele Colonna[1], Daniele D'Ercole[1], Girolamo Mincuzzi[1], Riccardo Riccitelli[3], Francesco Michelotti[2], Thomas M. Brown[1], Andrea Reale[1] and Aldo Di Carlo[1]
1 Centre for Hybrid and Organic Solar Energy Centre (CHOSE), Dept. of Electronic Eng., Tor Vergata University of Rome, Roma, Italy
2 Molecular Photonics Laboratory, Dept. of Basic and Applied Physics for Eng., SAPIENZA University of Rome, Roma, Italy
3 DYERS srl, Roma, Italy

2. Material and processing for dye solar cell technology

Since the introduction and development of the dye-sensitized solar cell (DSC) (O'Regan & Graetzel, 1991) several efforts have been made to optimize the materials involved in the photo-electrochemical process and to improve the light conversion efficiency of the device (Hagfeldt & Graetzel, 1995), by exploiting a low cost production process based on simple fabrication methods, similar to those used in printing processes.

2.1 Dye solar cells architecture and working principle

In Fig. 1 the basic configuration of a Dye Solar Cell (DSC) is sketched (Chappel et al., 2005). Amongst the main elements of this electrochemical photovoltaic device is a mesoporous nanocrystalline Titanium Dioxide (nc-TiO_2) film deposited over a transparent and conductive layer coated glass (in particular Soda Lime or Borosilicate). As alternative to the nc-TiO_2, other large band-gap semiconductors (such as ZnO, Nb_2O_5, and $SrTiO_3$) can be utilized as well as flexible and plastic (PET or PEN) substrates are a valid options in substitution of the glass. Generally, the nc-TiO_2 film thickness is fixed to a value comprised between few microns to few tens of microns and the substrates conductivity is provided by a transparent conducting oxide (TCO) coating. Fluorine doped tin oxide (SnO_2:F), FTO is the most commonly used (although Tin doped Indium Oxide (In_2O_3:SnO_2) ITO is frequently found onto plastic substrates) since enables low cost massive production of substrates showing a sheet resistance as low as 8 Ωcm^{-2} (Solaronix®).
On the surface of the TiO_2, a monolayer of visible light harvesting dye molecules is adsorbed resulting in the TiO_2 visible light sensitizing. A wide variety of dye molecules, included naturals dyes extracted from fruits flowers or leaves, have been proposed and tested (Polo et al., 2004; Kalyanasundaram & Graetzel, 1998). At the moment metallorganic ruthenium complexes containing anchoring groups such as carboxylic acid, dihydroxy, and phosphonic acid on pyridyl ligands show the best performances. Largely diffused are in particular dyes commonly named as N3, black dye, N719 and Z907, which enable fabrication of highly performing devices (Kroon et al., 2007; Nazeeruddin et al., 2005; Z. S. Wang et al., 2005).

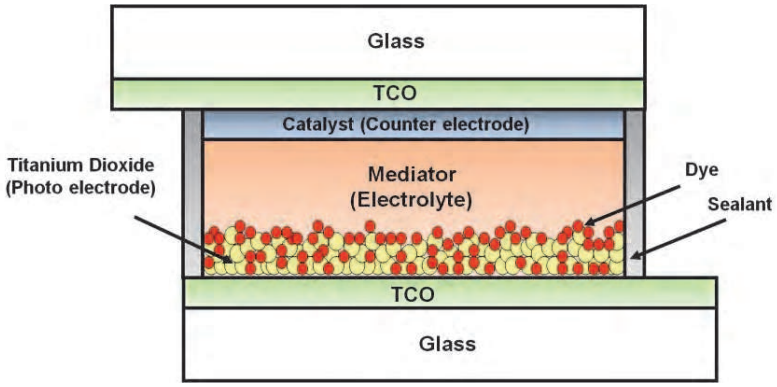

Fig. 1. Dye Solar Cell Structure. Basic cell's constituent are a transparent conductive substrate (TCO) coated glass and over it a nc-TiO_2 layer sensitized by a monolayer of adsorbed dye (photo-electrode), a red-ox mediator and, finally a catalyst (Pt) coated conductive substrate (counter-electrode).

It is worth to point out that the nc-TiO_2 mesoporous morphology (Fig. 2), for a film thickness of 10 μm, leads to an effective surface area about 1000 times larger as compared to a bulk TiO_2 layer, allowing for a significantly large number of sites offered to the dye sensitizer (Chen & Mao, 2007).

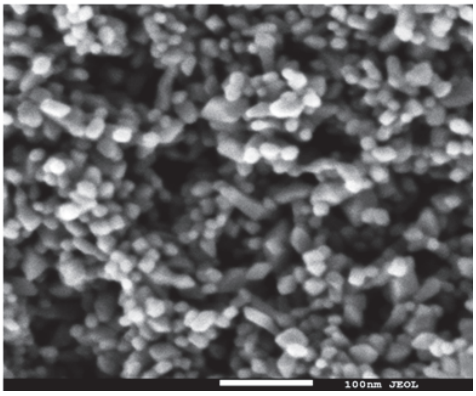

Fig. 2. A SEM image of nc-TiO_2 film utilized for Dye Solar Cells fabrication is shown. Although is possible to distinguish each nanoparticles (with a diameter of around 20 nm) large aggregates are evident resulting in a characteristic meso-porous morphology (Mincuzzi et al., 2011).

The conductive substrate together with the dye sensitized film form the cell photo-electrode. The dye sensitized film is placed in contact with a red-ox mediator electrolyte or an organic hole conductor material. The former is obtained solving a red-ox couple (such for instance the ions I_3^-/ I^- or $Co^{(III)}/Co^{(II)}$) in a solvent such as 3-me-thoxypropionitrile (MPN), acetonitrile (ACN) or valeronitrile (VN). Finally the device is completed with a counter-electrode generally composed of a transparent and conductive substrate on which a Pt film of few tens of nanometers is deposited for red-ox catalysis purpose. The two electrodes and the red-ox electrolyte mediator are sealed together, evoking the characteristic picture of a sandwich-like structure. The most diffused sealants are thermoplastic gaskets typically made of Surlyn® (i.e. random copolymer poly(ethylene-co-methacrylic acid) – EMAA), Bynel® (modified ethylene acrylate polymer) or alternatively vitreous pastes or glass frits.
Additionally, an optional light scattering layer made of particles with diameter of few hundreds of nanometers may be applied on top of the TiO_2 film in order to increase the photons optical path (transmitted light will be in fact back scattered into the nc-TiO_2 layer) and therefore the light harvesting (Hore et al., 2006). Although it has been demonstrated that this plays a beneficial role, a scattering layer leads to an opaque (not transparent) DSC device preventing the possibility of the use of the panel for building integration (as an active window for instance), one of the most interesting features and applications of DSC technology.
The working principle of DSC can be readily explained in terms of the electrons kinetics process and electrons transfer reactions taking place into the cell as a consequence of photon absorption. Fig. 3 shows the energy diagram and electrons transfer paths involved in a DSC.

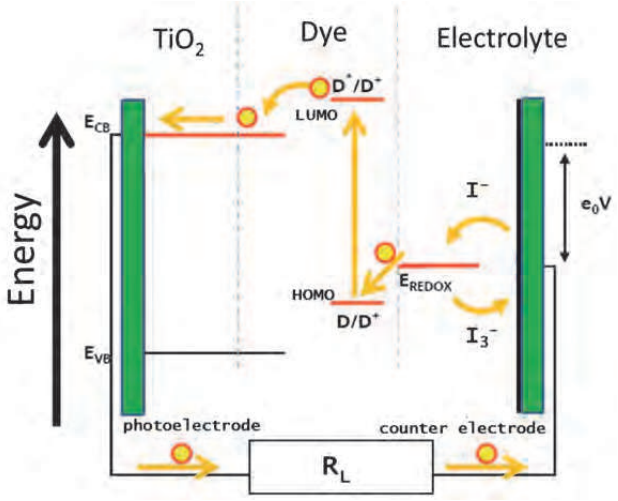

Fig. 3. DSC working principle: the absorption of a photon by a Dye molecule in its ground state D induce the transition to the excited state D*. The injection of an e^- into the TiO_2 conduction band occurs, resulting in the Dye oxidation D^+. The e^- diffuse into the TiO_2 reaching an external circuit and a load R_L where electrical power is produced. Successively it is reintroduced into the cell by the counter electrodes and regenerate the oxidized Dye D^+ utilizing a redox couple as mediator.

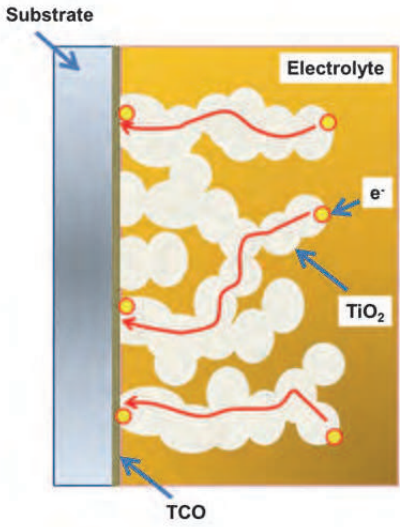

Fig. 4. The diffusion paths of the injected photon into the nc-TiO_2 conduction band are sketched. The nc-TiO_2 film sintering process promotes the electromechanical bonding between the nanoparticles facilitating the charge diffusion process in terms of increment of the intra-particles hopping rate.

By absorption of a photon, a dye molecule is set to the excited state D* from its ground state D. It follows that an electron is promoted from the highest occupied molecular orbital (HOMO) to the lowest unoccupied molecular orbital (LUMO) and then rapidly injected into the conduction band (E_{CB}) of the TiO_2. The dye molecule is then oxidized (D^+) whilst an hole is injected into the electrolyte. Charge transport occurs in the conduction band of the TiO_2 by pure diffusion of electrons percolating through the interconnected nc-TiO_2 particles to the FTO electrode (see Fig. 4). No electronic drift has been detected and electric fields in the TiO_2 are screened by the cations in the electrolyte, which penetrate the nano-scale pores of the TiO_2 (Van de Lagemaat et al., 2000).
Upon reaching the TCO electrode, the electrons are conducted to the counter-electrode via the external load (R_L) generating electrical power. Catalyzed by the platinum on the counter-electrode, the electrons are accepted by the electrolyte. This means, that the holes in the electrolyte (the I_3^-) recombine with electrons to form the negative charge carriers,

$$I_3^- + 2e^- \rightarrow 3I^-$$

By diffusion, the negative charge (I^-) is transported back with the aim to reduce the oxidized dye molecule (D^+). Triiodide (I_3^-) is formed and the electrical circuit is closed:

$$2D^+ + 3I^- \rightarrow I_3^- + 2D$$

Therefore, in DSC device charge separation and charge transport occur in different media spatially separated. Apparently the device generates electric power from light without suffering any permanent chemical transformation. Nevertheless, going in deep toward a device realistic and detailed modeling, processes involving current losses have to be included and remarked.
When a photon is absorbed, a dye molecule is set in an excited state S*, the back relaxation (or back reaction) into its ground state S may also occur, preventing the injection of an electron into the TiO_2 (see Fig. 5). As shown by Nazeeruddin et al. (Nazeeruddin et al., 1993) the injection process has a much larger probability to occur resulting in a characteristic injection time in the range of fs -ps, which is more than 1000 times faster than back relaxation (about 10 ns) straightforwardly negligible.
As reported above, electrons injected into the conduction band of the TiO_2 diffuse through the TiO_2 film toward the FTO anode contact. The electron transport into the mesoporous nc-TiO_2 film can be modelled as a combination of two mechanisms electron hopping between sites and multiple trapping/detrapping (Bisquert et al., 2009). In the latter case, electrons spend part of their time immobilized in trap sites from which they are excited thermally back to the conduction band. Nevertheless, during their transit, there is a significant probability that an electron recombine (and be lost) with the oxidized dye molecule S^+, before the dye reduction caused by the electrolyte. We are facing, nonetheless, to a process with a characteristic time of several hundreds of nanoseconds resulting 100 times slower than the reduction induced by the electrolyte (~10 ns) (Hagfeldt & Graetzel, 1995).
Instead, electrons injected into the TiO_2 conduction band may, during the diffusion, more often recombine with the holes in the electrolyte, i.e. I_3^-. This constitutes the most significant electron loss mechanism in the DSC and it can be asserted that the electrons transport by diffusion in the nc-TiO_2, and their recombination with the electrolyte are the two competing processes in the DSC technology, affecting the device efficiency of electrons collection (Peter & Wijayantha, 2000). It is important to point out that, although the triiodide concentration in

a DSC should be small for this reason, it should be high enough as to provide right amount of recombination for the electrons at the Pt counter-electrode. If this is not the case, the maximum current of the DSC will be diffusion-limited, i.e. cut by the diffusion of triiodide.

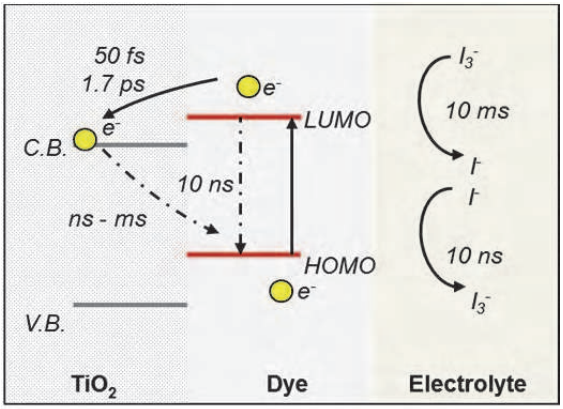

Fig. 5. Electron losses processes taking place into a DSC are shown. Also shown are the characteristic time relative to each of the considered processes.

Finally, it should be noted, that TiO_2 is a semiconductor with a large band gap of 3.2 eV, corresponding to a wavelength of λ=390 nm. Accordingly, visible light is not absorbed by the TiO_2 film. Direct absorption by UV-light is unwanted, since the created holes in the valence band of the TiO_2 are highly reactive and tends to produce the so called side reactions in the mediators, highly destructive for the long life time of the cell (Hinsch et al., 2001).

2.2 Dye solar cells fabrication

One of the main advantages connected with the DSC technology is the possibility to easily implement the fabrication steps involved, often borrowed from the printing industry, processing abundant materials with a relative low mass production costs (Di Carlo et al., 2008).

Differently from others photovoltaic technologies (those Si-based for instance) which are more mature and produced in an industrial environment according to well established procedures (Ito et al., 2007), for DSC a standard fabrication procedure is yet to be defined. Nevertheless the following steps are widely reported in literature, they strongly represent a prerequisite list to define and set-up an eventual industrial DSC pilot production line:

a - Cleaning of transparent and conductive substrates. Is generally carried out sonicating the substrates successively in solvents like acetone and ethanol for few minutes. In the case of glass substrates, this step may be further accomplished by firing the substrates in furnace or oven, in order to burn out the organic compound and preserve the subsequent processes.

b - TiO_2 film deposition. To obtain a mesoporous nc-TiO_2 film, from few micron up to few tens of microns thick, various techniques are adopted. One of the more diffused consists in preparing a colloidal paste composed of TiO_2 nanoparticles, organic binders, and solvents (Ito et al., 2007) and deposit it by various printing techniques such as screen printing, slot dye coating, gravure coating, flexographic printing, doctor blade and spray casting.

According to the printing technique performed, the composition of the paste and its recipe may observe some slight variation. For instance, in the case of automatic screen printer, it is recommendable to use TiO_2 pastes containing printing oil such as terpineol in order to facilitate the deposition process and a solvent like ethanol to optimize the deposition process for doctor blade technique. Also utilized are techniques such as spin coating, sputtering and electro deposition (Chen & Mao, 2007). It is interesting to point out that with the use of a layout or a mask it is possible to deposit the colloidal nc-TiO_2 layer according to a given pattern or shape.

Different authors have also shown the possibility to fabricate Dye Solar Cells utilizing TiO_2 films made with ordered nanostructures such as nanotubes, nanowires or nanorods (Chen & Mao, 2007). In these cases colloidal pastes are not anymore considered and furthers techniques are utilized. It is important to mention amongst the others, chemical vapor deposition, physical vapor deposition, sonochemical method and microwave method (Chen & Mao, 2007).

c - TiO_2 sintering. After the colloidal TiO_2 paste is deposited, a thermal treatment more often indicated as annealing, firing or sintering is required. In fact it is possible, via heat, to get rid of solvents and organic binders contained into the paste and in the meaning time to promote an electromechanical bonding intra-particles and between particles and the underlying substrate. This step clearly has a huge bearing on the film morphology and porosity which in turn determines the cells performances. At the end of the sintering process, a trade off is required between the necessity to guarantee a good electromechanical bonding and the requirement to keep a large porosity maximizing the sensitized surface area. Conventionally an optimum, depending on the paste composition, is obtained applying the photo-anodes (before the dye adsorption) to an increasing ramp temperature in an oven, furnace or hotplate with a final ~ 30 min step at 450–500 °C (Mincuzzi et al., 2009).

Although this procedure guarantees the fabrication of DSCs with good performances (included cells having the highest efficiency ever reported of approximately 12% over small area (Nazeeruddin et al., 2005; Buscaino et al., 2007)) it shows nevertheless some drawbacks. Since the nc-TiO_2 is heated with the substrate the mentioned conventional procedure is unsuitable for plastic substrates. For similar reasons DSC would not be integrated on the same substrate with others optoelectronic devices which would be destroyed by the high temperature. Oven and furnace are energetically expensive increasing the payback energy of the whole fabrication process. Finally, at 450–500°C conductive glass substrates could bend irregularly, preventing the possibility to fabricate large area DSC devices.

Alternative procedures have been proposed with the aim to overcome some of the mentioned drawbacks. For instance there have been several attempts to produce the TiO_2 film via low-temperature sintering suitable for plastic substrates (100–150°C) by utilizing a binder free colloidal TiO_2 paste. However, the devices with low-temperature sintered films were found to exhibit lower efficiencies than those with high-temperature sintered films. Pichot et al. (Pichot et al., 2000) have fabricated a flexible TiO_2 electrode that was spin coated onto indium–tin oxide (ITO)-coated PET substrates from an organic-free nc-TiO_2 colloidal suspension and then sintered at low temperature (100 °C) for 24 h. However, the overall device efficiency was relatively low (1.22%) under 1-sun illumination (100mW/cm^2). A mechanical compression of a surfactant free colloidal TiO_2 paste onto an ITO/PET substrate at room temperature has been demonstrated as an alternative sintering method for making plastic-based DSCs at temperatures between 25 °C and 120 °C. Utilizing this method,

conversion efficiencies approaching 3% under 100 mW/cm^2 were reported (Lindstrom et al., 2002). Zhang et al. have developed a low-temperature chemical method for the fabrication of mesoporous TiO_2 films grown on ITO/PET substrates at 100 °C using a hydrothermal synthesis with conversion efficiency of 2.3% under 1-sun illumination. However, this process is only capable of partial crystallization of the starting Ti salts, and thus might require a subsequent high-temperature (450 °C) heat treatment (D. Zhang et al., 2003). Also several optical methods have been proposed including the use of I.R. lamps (Pan et al., 2009; H. Kim et al., 2006; Watson et al., 2010; Uchida et al., 2004) treatments. Nevertheless all the mentioned attempts produced solar cells with limited efficiencies compared to cells where standard high temperature sintering is carried out.

d - Dyeing. The nc-TiO_2 sensitization by dye adsorption (or dyeing) is carried out following two different strategies. In a case, sintered films are soaked with the substrate in a solution of ethanol and dye for a time period varying from around 10h to around 1h, depending on the dye solution temperature which correspondingly could be fixed in the range from T ambient to maximum T=80°C (which is ethanol evaporation temperature). Successively, TiO_2 films and substrates are rinsed in ethanol.

In the other case, devices are first sealed by means of a glass frit (see the step 6 below) and then dyeing is carried out fluxing the ethanol/dye solution through the gap between the electrodes. This second procedure has been introduced by the group of Fraunhofer ISE (Hinsch et al., 2008).

e - Pt deposition and thermal treatment. A crucial step in devices fabrication is to obtain a catalyst layer showing an effective catalytic activity. The main catalyst layer is a thin layer of Pt (some tenths on nanometers thick). Although the Pt layer could be obtained by sputtering, more frequently it is generally attained after thermal processing or curing of a Pt based precursor paste or solution which has been previously deposited by screen printing, doctor blade, spin coating or other printing techniques over the counter-electrode substrate. A Pt-based catalytic precursor paste composition suitable for printing technique is obtained mixing an organic compound (e.g. terpineol), a binder or stabilizer (e.g. ethyl-cellulose) and a precursor (e.g. hexachloroplatinic acid H_2PtCl_6) (Khelashvili et al., 2006).

A less viscous alternative, suitable for brush processing or spin coating, consists of an hexachloroplatinic acid solution in 2-propanol (Gutierrez-Tauste et al., 2005).

The cure of the catalytic precursor layer is conventionally carried out utilizing an oven, furnace or hot plate in order to treat the layer to a curing temperature with a final step of 5 – 30 minutes at 400 – 500°C (Kroon et al., 2007; Solaronix®). Whilst an effective Pt-precursor curing is guaranteed by this conventional procedure, nonetheless, the required high processing temperature induces some drawbacks already mentioned and listed in the case of nc-TiO_2 sintering. Kim et al. (S. S. Kim et al., 2006) also reported on Pt counter-electrodes prepared by means of direct current and pulse current electro-deposition methods, which are relatively simple and low cost processes.

Moreover these techniques are hardly scalable on large area devices. Alternatively, other materials than Pt, processed at low temperature (<150 °C) could be considered. As reported by Murakami et al., use of Carbon Black could be a valid and low cost alternative, and a small area cell showing power conversion efficiency exceeding 9% has been reported (Murakami & Graetzel, 2008). The same authors reported also a cell with catalyst layer made of Polymeric material such as PEDOT. Saito et al. and Suzuki et al. reported the application of a chemically produced conducting polymer and carbon nanotubes used as counter-electrode (Saito et al., 2002; Suzuki et al., 2003; Saito et al., 2004). Although the fabrication

cost can be decreased in these cases, the conversion efficiency is still relatively low compared to a cell with a Pt based counter-electrode.

f - Device sealing. Ideally, device sealing should be long lasting, minimize as much as possible H_2O infiltration (detrimental for the dye), O_2 infiltration (it induces dye photo-catalysis) and electrolyte leakage, the principal cause of module contacts corrosion (Okada & Tanabe, 2006). The sealant has to be Pb free because Pb degassing results to be an hurdle for the Pt catalytic activity (Sastrawan et al., 2006). Find a sealing material and procedure fully satisfying all the mentioned requirement is still an open issue for the DSC technology.

Nevertheless, as already mentioned, two different strategies are generally adopted for this purpose, by using thermoplastic gaskets, or glass frits. In the first case the sealing is attained by thermal pressing the two electrodes with the gasket between them. Alternatively a lead-free glass frit paste is deposited between the two electrodes and then heated until it melts sealing the device (Sastrawan et al., 2006). The melting temperature varies upon the glass frit paste composition, although it generally exceed 400 °C. Whilst in the first case the process can be carried out having the photo-electrode already dye sensitized, this is prevented in the last case since the high temperature necessary for the glass frit melting will damage the dye molecules. As reported in the step 4, for this reason dyeing is in this case carried out by fluxing the dye solution (Hinsch et al., 2008).

g - Electrolyte injection. Finally, by back vacuum technique, electrolyte is injected into the sealed device through an hole drilled into one of the substrates. The hole is on end stopped by means of a glass patch. Further possibilities consist in fluxing the electrolyte (Hinsch et al., 2008) or in printing (before the device sealing) a previously gelificated redox mediator (P. Wang et al., 2003).

2.3 Large area devices

Large area dye solar cell devices are obtained interconnecting unit cells to form modules which could in turn be interconnected to realize a panel. The individual cells must not only be insulated from each other electrically (and this is performed via TCO laser scribing), but also electrolytically otherwise photo-induced electrophoresis would occur.

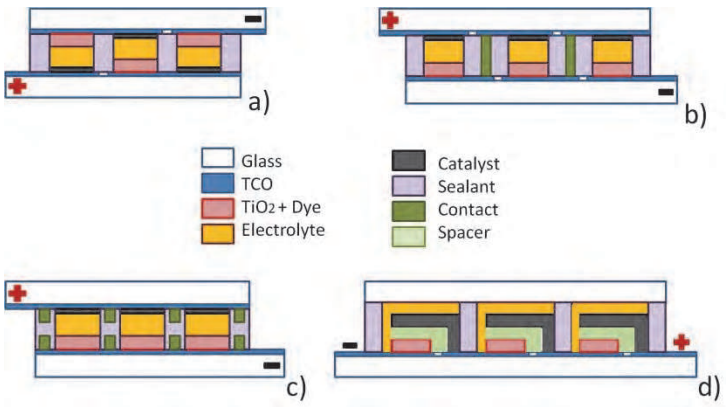

Fig. 6. Different architectures of Dye Solar Cells. Four different strategies are sketched: w-series interconnection (a), z-series interconnection (b), parallel interconnection (c), and monolithic-series design (d).

Furthermore, the electrical interconnections must be protected against the highly corrosive activity performed by electrolyte. As shown in Fig. 6 various interconnection architectures have been proposed for the modules, namely parallel, monolithic, z-series and w-series. Examples of modules obtained following different connections strategies are discussed in the literature (Tulloch, 2004) and disclosed in the following patents (Kay, 1995; Okada & Tanabe, 2006; Tulloch & Skryabin, 2006; Arakawa et al., 2007).

It is considered in particular modules to increase the voltage output cells which are connected together via either z-series or w-series schemes. In z-series design unit cells are sealed and connected by means of conductive vertical interconnections. The advantages of this design are an high voltage output and facility for eventual pre- and post-treatment of the electrodes. The disadvantage, is the risk of a fill factor lowering resulting from the series resistance of the interconnection. A crucial aspect regards the fabrication and realization of thermally stable vertical interconnections. Such interconnections need also to be protected from the corrosion eventually caused by the red-ox electrolyte leakage, which could compromise the modules performance and its working life time. An efficient and reliable interconnection strategy for z-series architecture modules is a still open technological challenge while some solutions have been proposed and disclosed in the following patents (Tulloch & Skryabin, 2006; Ezaki et al., 2006).

Differently from the z-series the w scheme avoids to interconnect altogether by juxtaposing cells facing in one direction with cells facing the opposite direction i.e. that have photo-electrode/counter-electrodes in opposite alternation and still requires separation of the cells by an effective sealing. This interconnection designs, is particularly attractive because the modules are potentially scalable to large dimensions avoiding the successive step of interconnection and integration of separate cells into a panel drastically simplifying the fabrication process compared to crystalline silicon panels. In DSCs the cells and interconnects can be integrated together by simple printing processes. Furthermore w-series design has advantages in simplicity and avoids the reduction in fill factor resulting from additional resistance of series interconnects, especially when the modules operate at high temperatures, but has some manufacturing and performance weaknesses. In manufacturing of this design, it is necessary that the counter-electrode and photo-electrode have to be processed on the same substrate. When conventional fabrication methods are utilized, this introduces processing complexities in deposition, curing, pre and post curing treatments of the cells materials in particular for the TiO_2 and catalyst precursor paste.

The design of a monolithic DSC (Vesce et al., 2011) is a planar-connected device with an only conductive glass, formed by a triple-layer sintered at once (Meyer et al., 2009) or together (Pettersson et al., 2007). The multilayer structure is typically composed by: a mesoporous TiO_2 working layer, a spacer/scattering layer and a counter-electrode layer. The spacer layer is often formed by ZrO_2 or rutile-TiO_2, while the counter-electrode layer is usually composed by Pt, Au, carbon or a mixture of these (Murakami & Graetzel, 2008). In order to obtain the maximum advantages from the monolithic architecture, some researcher reports the application of a quasi-solid gel electrolyte (non-volatile electrolyte) deposited by printing methods like blade-coating or screen-printing technique instead of an electrolyte processing by liquid injection (volatile electrolyte) (P. Wang et al., 2003).

For all types of serial DSC architectures, single cells must be insulated and serial connected causing a complex fabrication process, high serial resistance and a strong precision in order to maintain the ohmic contact (L. Wang et al., 2010). In contrast, a simple fabrication process is used to fabricate large scale parallel design DSC modules. In this architecture, (Tulloch,

2004), the grids utilizing conductive fingers to collect current are printed on the two substrates separately. Nowadays, the researchers that work on this design are devoting to find alternative materials solutions for the grid since Ag, Au, Cu, Al, and Ni are all easy to be corroded by the iodide electrolyte (Goldstein et al., 2010). Moreover, new coatings like polymer or glass frits are successfully applied in parallel DSC module design.
Having in mind the materials, strategies and fabrication processes aforementioned, various research groups (CHOSE, ISE Fraunhofer, KIST, NREL) and companies (3GSolar, G24i, Sony, Fujikura) have shown DSC panels and large area devices utilizing fabrication process which could be potentially integrated into an automatic production line.
Nevertheless, the scale up of DSC devices over large area for industrial and commercial purpose, poses some scientific and technological challenges. In particular, it is important to mention the reduction of the series resistance (Dai et al., 2005), strictly related to the increasing of the performance, stability and working life time of large area modules (P. Wang et al., 2003; Sommeling et al., 2004; Kuang et al., 2007), and the setting-up of a highly automated and energetically efficient fabrication process (Somani et al., 2005; Meyer et al., 2007; Mincuzzi et al., 2009).

3. Characterization techniques

The typical parameters to characterize a PV device belong also to DSCs performance. However, different technologies often imply different attentions to perform the measurement. Parameters like short circuit current, open circuit voltage, fill factor and power conversion efficiency, are extracted from the photo-current/voltage characteristic (J-V curve). This measurement can be fundamentally performed in two ways: in dark conditions (without illumination) and with illumination. In the last case, we are able to extract all the parameters. Illuminating with white light, the J-V curve represents an integrate response of the cell to all the wavelengths simultaneously. The standard test conditions (STC) correspond to power density of 1 sun (100mW/cm^2), light spectrum of an air mass 1.5 global (AM1.5G) and working temperature of 25°C.
Incident Photon-to-electron Conversion Efficiency (IPCE) measurements, on the other hand, quantify how many incident photons at a single wavelength are converted in extracted electrons at the electrodes. It strictly depends on the optical and electrical properties of the cell. In particular, it can be decomposed in the product of three main terms: light harvesting efficiency (LHE), injection efficiency (η_{inj}) and collection efficiency (η_{col}) (Halme et al., 2008; Barnes et al., 2008). The first is reduced by optical phenomena, such as reflections, transmission and competitive absorption, while injection and collection efficiencies depend on electrical mechanisms at widely different time scales. The injection counts how many excited electrons are transferred from dye molecules to titanium dioxide film. It is the fastest process in the cell, with characteristic times from femto to pico-seconds, measured by means of pump-probe techniques (Koops & Durrant, 2008).
The collection efficiency says how many injected electrons into the titanium dioxide film reach the electrodes. It can be evaluated by many different techniques, among which photovoltage decay (Walker et al., 2006), intensity modulated photovoltage spectroscopy (IMVS), intensity modulated photocurrent spectroscopy (IMPS) (Schlichthorl et al., 1999) and electrochemical impedance spectroscopy (EIS) (Q. Wang et al., 2005). The slowest process in the cell is the ionic diffusion in the electrolyte, which can be studied by EIS as well.

3.1 I-V characteristics and IPCE spectra

I-V characteristics and IPCE spectra can be related each other. Actually, from the complete IPCE spectra, it is possible to calculate the short circuit current that one should measure under solar simulator in the following way:

$$J_{SC}(\lambda) = \int_{\lambda 1}^{\lambda 2} IPCE(\lambda) P_{STC}(\lambda) \frac{\lambda}{1240} d\lambda \quad (1)$$

with $P_{STC}(\lambda)$ the spectral density at standard test conditions and λ the wavelength in nm. This calculation is an important check that should be always performed to control the measurement accuracy. Many factors can influence the deviation of the current measured under solar simulator from the value calculated by equation (1). In particular, according to the solar simulator class, the spectrum can considerably differ from AM1.5 conditions (Ito et al., 2004). Because the calculation is performed at AM1.5, an overestimation or an underestimation can occur. It mainly depends on the light harvesting efficiency of the cell or more simply from the absorption coefficient of dye molecules. A good way to overcome this discrepancy consists in estimating the mismatch factor (M) (Seaman, 1982). It considers the spectral responses of the test and reference cells and the spectral irradiance of the solar simulator (while AM1.5 is known). It can vary a lot among various kind of cells (it is close to unity for silicon solar cells). In Fig.1 the calculated and the measured currents for dye solar cells with different dyes are put in relation. Different dyes mean different absorption spectra, and consequently a variation of the mismatch factor. Although a linear relation is obtained, the angular coefficient is different from one. Moreover, to make the things more complicated, there is the dependence of dye solar cells response from the level of illumination. So, as it will be clear soon, to relate the results from IPCE and J-V measurements is important to be in the same light intensity conditions. It means that also IPCE spectra should be acquired at 1 sun condition.

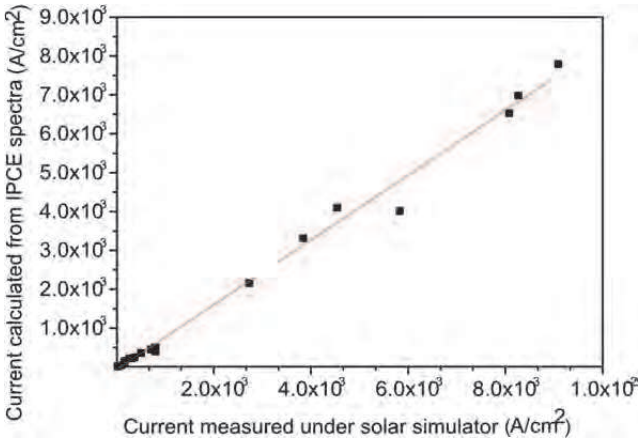

Fig. 7. Density Current measured under solar simulator and calculated by IPCE spectra are put in relation for cells with different dye molecules. A perfect agreement would give an angular coefficient m equal to one. In this case we have m=(0.83±0.02) and an adjusted R-square of 0.992.

Actually, DSC photovoltaic characterization is critical. Performing J-V curve, the direction of scan as well the delay time during the measurement must be chosen accurately otherwise different results can be obtained. One of the most important reason for these different behaviors is due to strong capacitance effects presented in this kind of device (Koide & Han, 2004). The main consequence is the long constant time of this kind of cells (in the order of some seconds) with respect to other technologies. An overestimation of short circuit current can be carried out, in particular when small area cells are characterized. In this case, the device area is generally larger than the active area, and, when illuminated, a considerable amount of light not impinging onto the active area can be redirected to it (light piping effect) (Ito et al., 2006). According to the simulator class, the beam divergence can amplify this effect. To overcome it, an appropriate opaque mask must be applied onto the external surface front glass. Then, particularly for large area devices, or for devices delivering high current, the external bad contacts can strongly influence the measurement. Good contacts can be obtained with bus bars applied by screen-printing technique.
On the other hand, IPCE measurement on dye solar cells is a critical issue as well. IPCE measurements can be performed in two ways, applying a direct (DC) or an alternate (AC) method. The first one is the classical way to acquire IPCE spectra, while the second one consists in illuminating the cell with white light (also called bias light) simultaneously with the monochromatic component. The bias light acts as a sort of polarization of the cell, increasing its response, besides the fact that, in this way, the cell can be put under conditions closer to the working ones. The current due only to monochromatic light (we say monochromatic current) is discriminated from the current due to the bias light, by using a coherent detection. It means that the monochromatic light is modulated at a certain frequency and by a lock-in amplifier, only the current modulated at the same frequency will be detected.

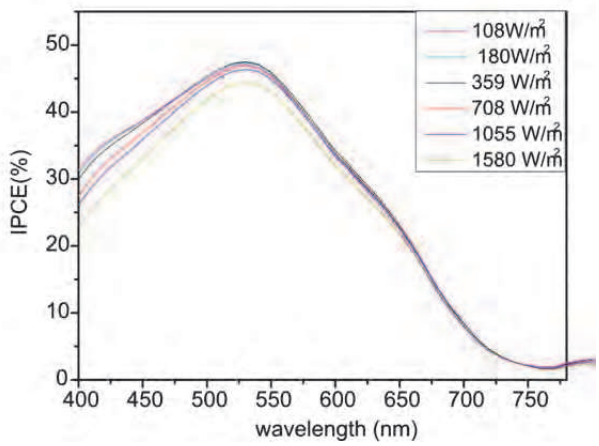

Fig. 8. IPCE spectra in function of the bias light illumination. A clear dependence from the light power density is shown. In the legend, the bias light power density is shown.

There are mainly two effects affecting IPCE when we illuminate with different power density conditions: the trap filling effect and the electrolyte ions mobility. While the first affects negatively the IPCE spectra at low light level conditions, the second comes into play at high light density reducing the solar cell response as well. For trap filling we mean the ability to occupy the states inside the titanium dioxide gap, close to the conduction band edge. These levels are centers of recombination for the electron in conduction band. At single wavelength, the filling is not efficient, reducing the cell response (see Fig. 8). It has been verified that the application of a bias light can be simulated in the DC method, if the intensity of the monochromatic light is high (Sommeling et al., 2000). On the other hand, at high intensity the electrolyte ions could be not able to regenerate effectively the homo level of the dye. This effect is dramatically enhanced when we use $Co^{(II)}$-$Co^{(III)}$ as redox couple.
Aware of the dependence from light intensity, to control the measurement accuracy under solar simulator, it is mandatory to perform IPCE acquisition at the same conditions.
Different dynamics are present in the photovoltaic mechanism of a dye solar cell. In presence of illumination, however, only the slowest process will dominate. The result is that the dye solar cell response is really slow. The modulation of the monochromatic light should be less than 1 Hz, taking into account that it should be verified every time different materials are involved (in particular the electrolyte and the titanium dioxide film employed).

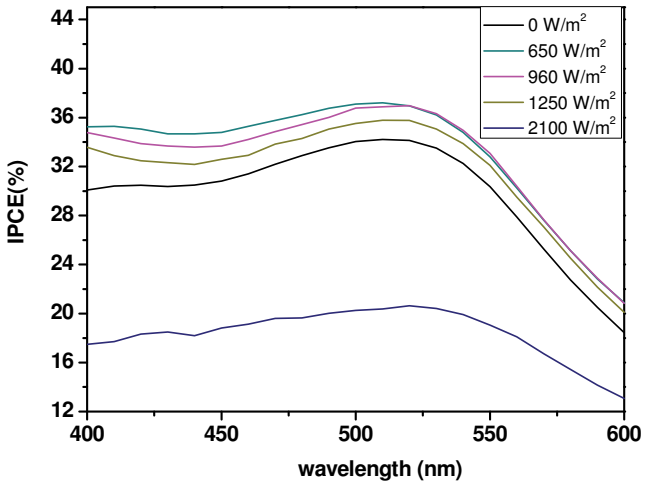

Fig. 9. IPCE spectra in function of the bias light illumination for a dye solar cell with $Co^{(II)}$-$Co^{(III)}$ as redox couple. A decrease of the signal intensity at high intensity levels has been measured.

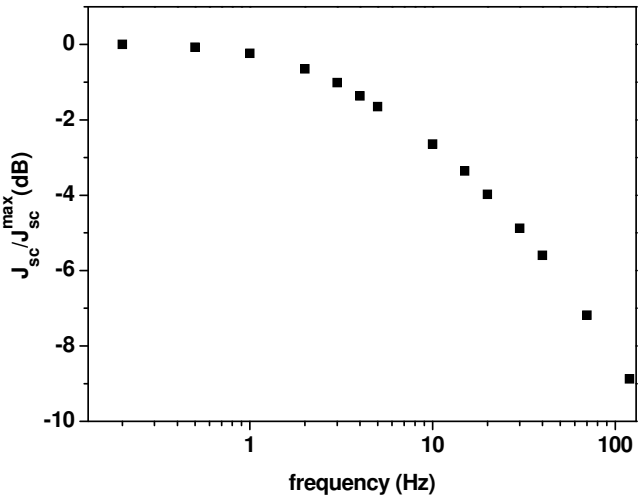

Fig. 10. DSC response in function of light frequency modulation. In the y-axis, photocurrent appears as a ratio (in decibel) with respect to the maximum current at the lower frequency. The response of a DSC is slow if compared to silicon technology.

IPCE spectra take in account many different phenomena that we can distinguish in two main categories: optical and electrical ones. In particular IPCE depends on the ability of the cell to harvest the light. Photon management techniques try to improve just this factor. The light harvesting efficiency of the cell can be calculated starting from spectrophotometric measurements. A simple optical model of the geometry allows the estimation of this quantity, that is the electrons generated compared to the incident photons. In a simplified scheme, assuming a Lambert-Beer behavior, we can model the light harvesting efficiency when the light impinges onto the front side of the cell in the following way:

$$LHE(\lambda) = T_{TCO}(\lambda) \cdot \frac{\alpha_{dye}}{\alpha} \cdot \left(1 - e^{-\alpha d}\right) \tag{2}$$

where T_{TCO} is the transmittance of the transparent conductive oxide, α is the absorption coefficient of the entire film and α_{dye} is the absorption coefficient due to the dye molecules. This is, obviously, a simple approach, where second-order reflectance terms are not considered. Measuring IPCE and estimating LHE, we are actually able to obtain information about injection and collection efficiencies just making the following ratio:

$$APCE(\lambda) = \eta_{inj}\eta_{col} = \frac{IPCE(\lambda)}{LHE(\lambda)} \tag{3}$$

where APCE stands for Absorbed Photon to Current conversion Efficiency and it is the product between injection and collection efficiencies.
Making the measurements illuminating both sides of the cells in different times, an estimation of the collection efficiency, the diffusion length (L_D) and the injection efficiency, has been demonstrated under strict conditions (Halme et al., 2008; Barnes et al., 2008).

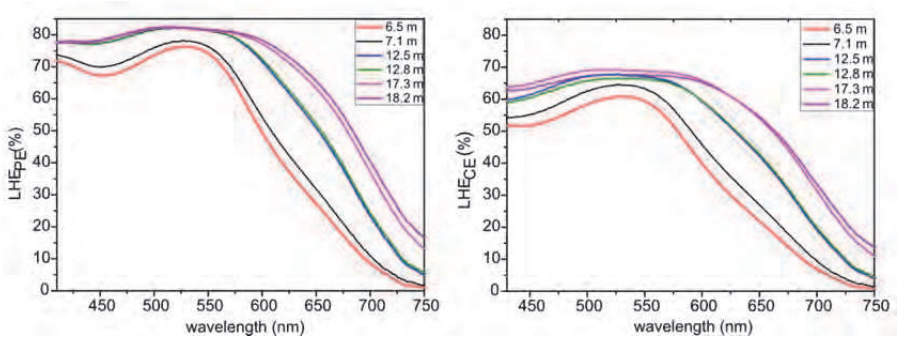

Fig. 11. Light Harvesting Efficiency for cells with different thicknesses illuminating from photo- (on the left) and counter- electrode (on the right) sides.

In Fig. 11, estimation of LHE for different thicknesses of the titanium dioxide film for both directions of illumination has been reported. As intuitive, LHE from counter electrode side is typically less than in the case of front side because of the generation profile inside the titania layer and the electrolyte absorption, mostly in the wavelength range under 500 nm.

4. Photon management

The typical paths followed to increase the performances of DSCs are linked to their main components, i.e., to improve the mesoporous nanocrystalline titania (nc-TiO_2), to find new dyes or dye combinations and to improve the ionic electrolyte. Approaches to enhance efficiency are also being followed which belong to a wide strategy of photon management. The dye management itself acting on the dye properties may be considered inside the panorama of photon management (Park, 2010). It consists in a multiple dyes co-sensitization in order to enlarge photonic response via panchromatic absorption, hence to increase efficiency. There have been already proposed works focalizing on the panchromatic feature of a dye solar cell (Ogura et al., 2009; Yum et al., 2007; Park, 2010). The way to get improvement is by the use of two (up to three) dyes adsorbed on the nanocrystalline titania that are responsible for broad spectral response of the device. The development of organic sensitizers (C101 etc.) (C.-Y. Chen et al., 2007; Abbotto et al., 2008) led to very high levels of efficiency. More in general, photon management consists in the ability to confine light in the dye solar cell to stimulate high levels of charge enforced by scattering and reflection effects. At the same time, this should be coupled to decreasing the recombination of charge mostly at the interface nanocrystalline TiO_2/electrolyte. Indeed, it is known that the top performances of DSC devices are reached by keeping in mind also all the parasitic and recombination effect and the way to minimize them. For example, in order to quench the recombination at FTO/electrolyte interface and to facilitate the injection between the dye LUMO and the TiO_2 conduction band, it can be used a photoanodes treatment by a titanium tetrachloride (TiCl4) solution (Vesce et al., 2010). Then, the transparent layer of titania (average particle diameter 15-20 nm) can be covered or added by larger scattering particles (150-400 nm in size) (Usami, 1997; Arakawa et al., 2006; Colonna et al., 2010) causing the random reflection of the light back into the cell (Mie scattering). Indeed, the most common way of photon management consists in the development of diffuse scattering layers (SLs) capable to be used as incoherent back mirrors for the incoming light passing through the cell

and otherwise not converted into current. In 1997 (Usami, 1997) a theoretical work by A. Usami proposed the use of a scattering layer onto the nc-TiO_2 layer and a rutile thin layer between the glass and TCO conductive film. This implies a very effective enhancement of the light collected into the cell, but also means that the DSC remains opaque. Nowadays, the scattering layers (Hore et al., 2006; Arakawa et al., 2006), centers (Hore et al., 2005) and superstructures (Chen et al., 2009; Q. F. Zhang et al., 2008) are well known and routinely used (Graetzel, 2005). Despite other approaches to the problem of increasing DSC performances while maintaining light transmittance (Colodrero et al., 2009a; Ogura et al., 2009) the record of performance for a DSC is obtained by the use of diffuse SLs (Nazeeruddin et al., 2005; Arakawa et al., 2006). To confer order to the scattered light, Miguez proposed the selective mirror for DSC (Colodrero et al., 2009a) made out from colloidal TiO_2 suspensions (Wijnhoven & Vos, 1998; Colodrero et al., 2008). They consist in photonic crystals (PCs) (Yip et al., 2008; Colodrero et al., 2009b), introduced either inside the titania layer or on its backside (Nishimura et al., 2003; Mihi et al., 2006), currently under an intense experimentation. Scheme in Fig. 12 resumes some of the light management approaches for conversion efficiency improvement.

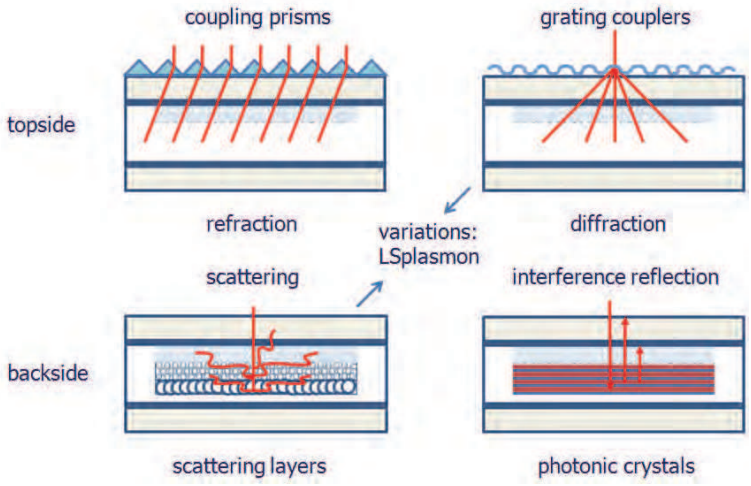

Fig. 12. Photon management basic approaches.

Some of these techniques will be described in the following sub-sections. In both SLs and PCs techniques of photon management, the increased light path in the active layer (e.g., by scattering or interferential confinement), will enhance the light harvesting efficiency (LHE). Even the reflection can be exploited to call into play of photons otherwise lost from the cell, as in V-shaped or folded solar cells (Tvingstedt et al., 2008; Zhou et al., 2008). In the waveguide DSC (Ruhle et al., 2008) a coupling prism let the light enter beyond the condition of total reflection at the glass plates/air interface without letting it to escape. Plasmonic solar cells (Tvingstedt et al., 2007; Catchpole & Polman, 2008) may represent another kind of photon management for field enhancement (near-field) or scattering by surface plasmon polaritons (mostly localized on metallic nanoparticles). Other

configurations involve field enhancement plus diffraction from metallic subwavelength arrays (Hagglund et al., 2008; Pala et al., 2009; Ding et al., 2011). An increased optical path may be obtained in principle also by dielectric diffraction or refraction (Dominici et al., 2010). Structuring the top side with a dielectric surface texturing, either nanometric or micrometric (Tvingstedt et al., 2008), could achieve the additional (diffracted) light rays or a larger inclination of (refracted) path (respectively by using of grating couplers or microprisms and microspheres for example).

4.1 Co-sensitization

The co-sensitization of nc-titania anodes approach consists in the use of two or more dyes anchored on the same substrate (Chen et al., 2005; Shah et al., 1999). It has been considered with particular attention to some organic dyes having complementary spectral response in the red with respect to the ruthenium-based dyes (largely used for standard DSC), such as squaraine (SQ1) (Clifford et al., 2004), cyanine (Pandey et al., 2010), phthalocyanine (Ono et al., 2009), hemicyanine (Cid et al., 2007). Indeed in other studies the co-sensibilization approach has shown high device performances toward red and violet as well in the electromagnetic spectrum (Yao et al., 2003; Kuang et al., 2007; Yum et al., 2007, 2008; Chen et al., 2005; Clifford et al., 2004). The scope of co-sensitization is to enlarge the absorbance spectrum of the cell toward the Near Infra Red (NIR), thus to increase the Incident Photon to Current Efficiency (IPCE) by enhancing the LHE (*Light Harvesting Efficiency*) and the efficiency of injection inside the TiO_2 (see IPCE section).

Here have been investigated the co-sensitization effects by using two conventional Ru-based dyes, the N719 and the Z907, together with a second one that is a typical Dye for dye lasers (HWSands). With respect to other co-sensitization approaches it has been shown the improvement of performances without losses when the dyes are both anchored to TiO_2. This means that the behavior of photocurrent and efficiency is summed not linearly, i.e. more than the sum of each single dye performance cells.

The most important fact to take into account in this approach is that the dye does not reach the saturation point, i.e. maximum allowed absorbance and hence maximum performances. What done is the immersion by using the first ruthenium dye followed by the second one for a determined time. In fact by setting properly the dipping time there have get enhanced performances with respect to 'one dye system DSC'. It should be noted that the immersion time far from the saturation of the titania layer for the ruthenium dyes implies technological reasons. In fact in Building Integrated Photovoltaic (BIPV), to which DSC are devoted, the transparency is a central factor. A saturated working electrode will be slightly opaque, while by using a second dye absorbing toward the red together with the unsaturated one is possible to keep an acceptable level of transparency and efficiency.

Experimental spectra were acquired with the integrating sphere of a Spectrophotometer by using the undyed titanium dioxide substrate as reference. The working electrode's absorbance saturates after some hours for N719 and Z907 depending on the thickness of TiO_2 and dye concentration whereas for SDA is found that the saturation time is of the order of 15-30 minutes for both thicknesses investigated and has been also observed a photo-cleavage due to TiO_2. In the figure below are reported absorbance of N719 on nc-TiO_2 at different times and the photocatalisys of NIR dye.

The optical response of the double dye is enlarged up to 700nm due to the presence of near IR dye. It should be noted that prolonged dipping time in the SDA solution will cause a displacement towards the N719 molecules already attached on the TiO_2 surface; in fact MLCT (Metal to Ligand Charge Transfer) band absorption of N719 (3h) decreases after 15 minutes dipping in SDA. The same trend is kept also for 30 and 45 minutes (see Fig. 14).

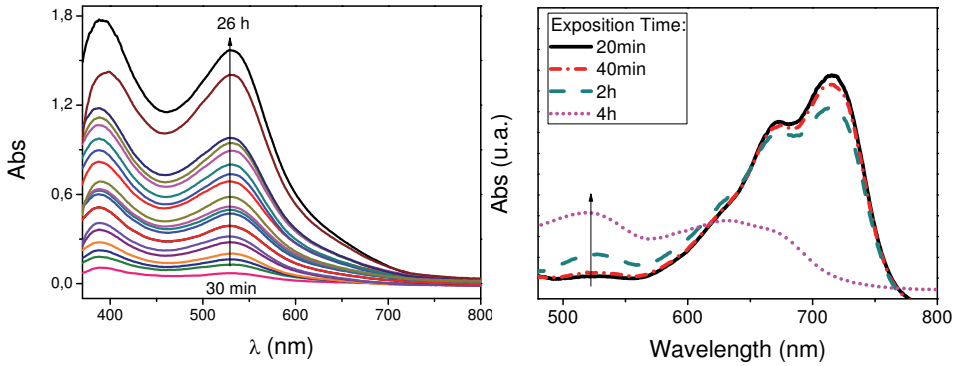

Fig. 13. (Left) Absorbance of nc-titania dyed with N719 (30 min up to 26 hours) and (right) photo-cleavage of SDA due to the TiO_2.

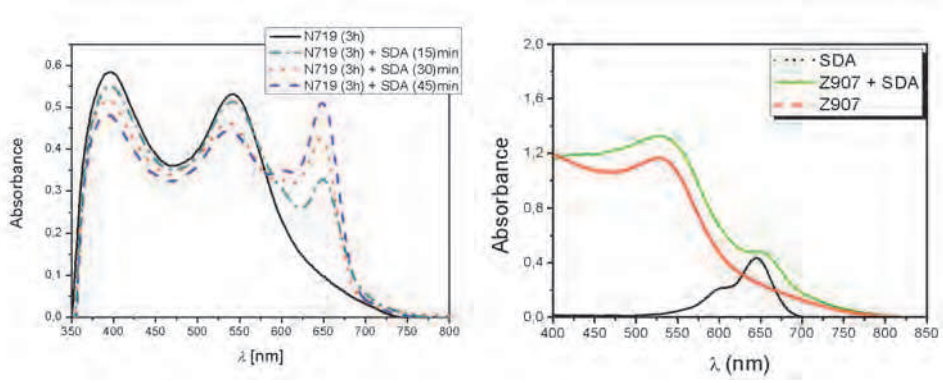

Fig. 14. Left: Co-sensitized spectra of the SDA1570 dye together with N719 on nanocrystalline titania substrates (6 μm) along with single dye absorbance. Several dipping times were chosen to show the decreasing peak of the N719 due to SDA1570 effect. Right: Co-sensitized spectra of the SDA1570 dye together with Z907 on nanocrystalline titania substrates (12 μm) along with single dye absorbance.

There is the gradual detaching of the N719 molecules from the titania due to the SDA environment. In this process it should be considered the equilibrium constants of the process involving initially the N719-TiO_2 photoelectrode in EtOH solution of SDA. The latter molecules act on the substrate by mass action due to the concentration gradient. The SDA molecule acts for N719 detaching from the TiO_2 surface. This depends mainly on the concentration of SDA solution, on the temperature, and the time. Finally there will be reached a dynamical equilibrium in which the number of SDA entering molecules on titania is equal to the same detaching molecules. Since such configuration is undesired, the finding of the optimal adsorbing point by both N719 and SDA molecules is central factor.
For completeness the action of SDA on dyed N719 PEs and *vice versa*, immersed up to 18 hours on titania was investigated (see figure 15, right). It is found that SDA is not able to detach all the N719 molecules, consequently the absorbance has almost the same trend for

15 minutes and 18 hours of SDA on saturated (18 h) N719 PE. The N719 instead shows an increasing of the absorbance passing from 15 minutes to 18 hours when alone (figure 15, left); moreover the attachment dynamic of N719 is very slow if compared to SDA. On the contrary it can be seen that the N719 environment for a saturated SDA photoelectrode is deleterious for the latter, being completely cancelled (figure 15, dot curve). It can be noted that the maximum absorbance of N719-SDA PEs is almost the same for 15 minutes and 18 hours of SDA immersion meaning that the affinity of SDA to the N719 saturated titania is limited.

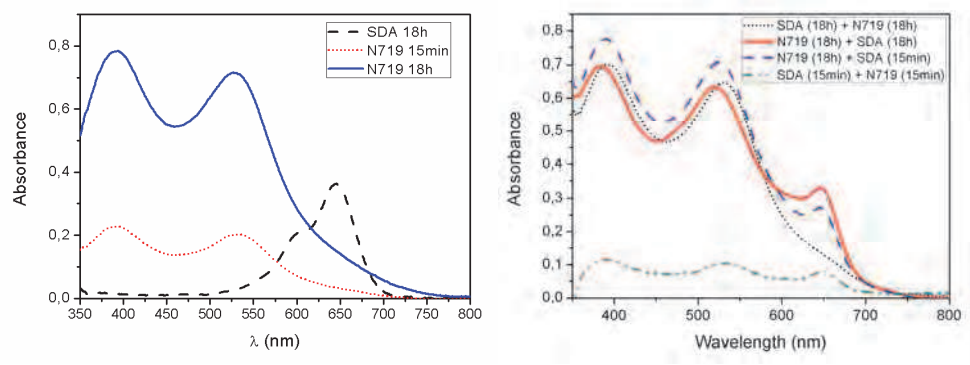

Fig. 15. Absorbance of 6 micrometers titania PEs in several dye adsorption configurations; (left) single dye TiO_2 attachment and (right) saturation conditions.

A similar study for Z907 + SDA system has been carried out; the transparent 12 micrometers thick TiO_2 PE was dipped in Z907 (0.3 mM) for 5 hours, while SDA for 30 minute steps. In this case, due to the ability of the thicker PE to generate an higher current with respect to the previous case, the electric performances are notably higher than N719 (Fig. 16).

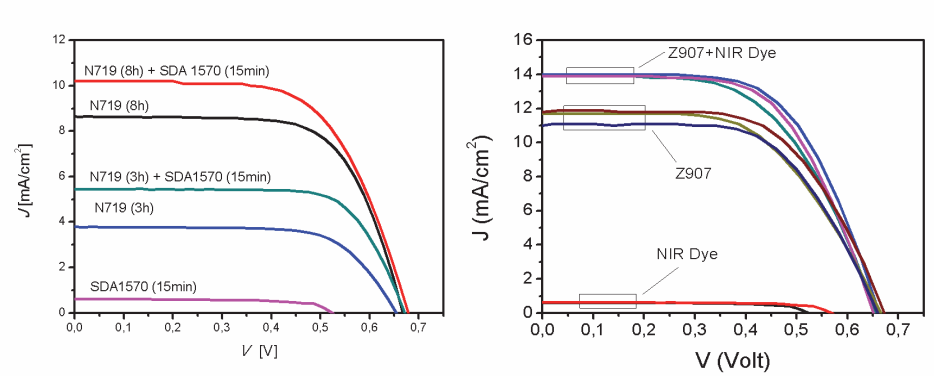

Fig. 16. J-V curves for N719-SDA (left) and Z907-SDA (right) co-sensitized systems. The lowest curve is due to the SDA sensitizer alone (labeled NIR in the right plot). It can be seen that the contribution of SDA is very small when compared to the N719 or Z907 current generation, but it becomes very important when the ruthenium dye is already and partially attached to the surface.

In this case, by taking into account that the Z907 Ruthenium-based dye has hydrophobic chains, we shall consider that (relatively) prolonged dipping times are required by the SDA to attach efficiently to the Z907 dyed titania PEs. This explains the small absorbance seen in figure 1 where the Z907 (5h) is immersed for thirty minutes in SDA solution.
The cells assembled by using the above photoanodes arrangements have been tested under a sun simulator (AM1.5) at 0.1Wcm^{-2} of illumination density of power. It is found that for N719-SDA system (at different dipping times) the co-sensitized cell outperform the single dye, having unexpected Jsc generation and efficiency. The same trend, but with higher values, has been found for Z907-SDA arrangement.
The Internal Photon to Current Conversion Efficiency confirms the above trends showing a zone of generation at the SDA excitation energy (650-660 nm).

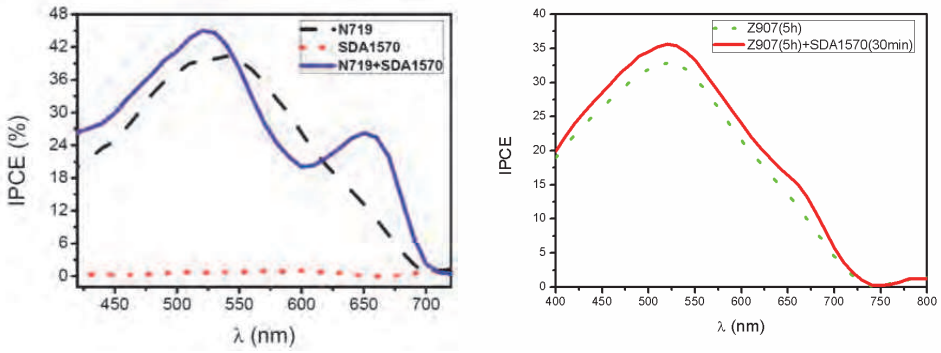

Fig. 17. IPCE results of the studied systems. In the case of N719-SDA couple the SDA pick is well identified at 660, whereas in the Z907-SDA only a small increasing of the IPCE figure is registered.

The immersion of the partially N719-sensitized photoanode in a SDA solution induces the saturation of the remaining free TiO_2 surface and at the same time a partial displacement of the already attached N719/Z907 molecules, creating a sort of "self-organization" of the two molecules that improves the cell performance, limiting the energy loss due to excitonic interaction between homologue molecules. This seems to be confirmed by IPCE measured. It shows in fact that photocurrent for the co-sensitized cell has a relative maximum in the wavelength region of maximum absorbance of SDA1570 confirming that it acts as an absorber on the TiO_2 but not as carrier generator in the cell when anchored alone to the titania. Instead, if attached together with N719 a major contribution in charge collection starts. Moreover the N719 active spectra in the co-sensitized device is blue shifted and narrower than that in the non co-sensitized device. Such a molecular organization effect can justify the fact that SDA1570 alone is not a sensitizer, while together with N719 it becomes a sensitizer for DSCs (Colonna et al., 2011a).

4.2 Diffusive scattering layers

The use of larger titania particles dispersed or added in layers on the nc-TiO_2 slab of a dye solar cell has been proven to be the best arrangement for high performance DSC (Nazeeruddin et al., 2005). The scheme of a DSC having a thin slab of opaque titania

particles (~ 150-400 nm) onto the transparent one in several configuration is depicted in Fig. 18. The optimal diameter of the transparent nc-titania particles is about 15-20 nm; during the sintering process at nearly 500°C, the particles create the mesoscopic structure and the effective surface of the TiO_2 electrode is increased by up to 10^3 factor with respect to the apparent area. In this way when the dye is adsorbed there are up to 1000 monolayers of dye in the cell for charge generation (Ferber & Luther, 1998). The pores in the layers have the better diameter for electrolyte infiltration and diffusion. If the TiO_2 particles are too small, the pores are not large enough for the dye and the electrolyte infiltration. Finally the larger the size particles the smaller is the internal surface, hence poor charge generation.

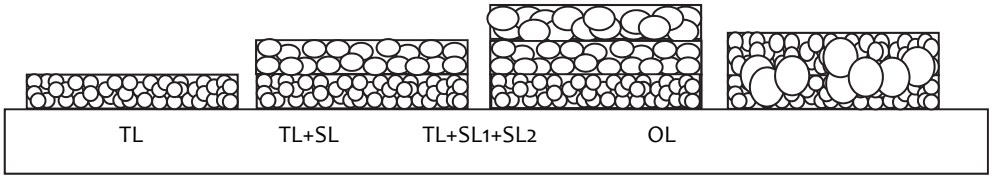

Fig. 18. From left to right hand: few micrometers nc-TiO_2 (~ 15-20nm); single scattering layer (d ~ 100nm) on the previous; double scattering layer with upper one having d > 200nm particle size; dispersion of small and large diameter TiO_2 particles. TL = Transparent layer, SL = Scattering Layer, OL = Opaque Layer.

Due to the opacity of scattering titania particles placed onto the transparent nc-TiO_2 the incident light passes through the nanocrystalline dyed titania, then it encounters the diffusive slab of bigger particles and is resent back to the PE finally. The average size of the scattering particles can be tailored to be between 60 and 500 nm, whereas the layer thickness can vary between 3-4 and 20 micrometers (Arakawa et al., 2006; Koo et al., 2008).
It should be considered that by doubling the thickness of nanocrystalline transparent titania the photocurrent will not be doubled because the difference in transmittance decreases with increasing wavelength, that is, little difference at wavelength ranging from 650 nm to 800 nm. For this reason, a TiO_2 film having only nanocrystalline particles cannot improve photocurrent density significantly by increasing the film thickness (Park, 2010). For this reason the random effect of a diffusive layer can enhance the reflectivity back to the cell by increasing the incident light path length and therefore the absorption, thus the LHE. All the works based on such strategy have been based on *A. Usami* (Usami, 1997) studies to demonstrate that with a simple model for multiple scattering the best configuration can be obtained with particles which size is a fraction of the incoming wavelength. *Usami* considered that Mie scattering theory is a rough approximation if scattering particles are not spherical and for multiple scattering. To take them into account some corrections have to be introduced. The exact solution of scattering of light by a particle is obtained by Mie theory, along with the dependence on particle size, absorption index, uniform dispersion of the particles, sufficient particle condensation for effective electron transfer and sufficient opening for the adsorption of the sensitizers (Arakawa et al., 2006; Park, 2010).
It has been found that the optimal scattering matching condition is obtained for $kd/\pi = 0.7 \sim 1.6$. Since the wave vector is given by $k = 2\pi/\lambda$, this condition implies that it exists an interval of wavelengths and size scattering particles for best improvement condition.
For this study it has been investigated firstly the absorption, i.e. A = 1 - T - R, of substrates taking into account the reflections of the device. In this way can be understood the spectral

area in which the diffusive layers can efficiently operate. In the figure below can be seen the absorption of nc-TiO_2 of 6 and 12 μm along with the SLs effect. It should be noted that the growth of 1 or 2 diffusive slabs of the same particle diameter creates the same absorption to the PE.

For quantitative estimation on the cell performance the study the IPCE trend of the cell is required in order to see explicitly the enhancement factor. This is because the absorption curve does not take into consideration the final device arrangement, that is the current generated by itself. On the right plot of the figure are shown reflectance spectra (diffuse and specular) due to transparent or scattering particles, in a normal configuration. Typically the SL can enhance the photocurrent to very high percentage because of the random reflection. Indeed it can be seen that almost all the reflected light by the scattering layer is intercepted by the dye pigment up to 600 nm. Therefore the absorption A of the cell will be increased as the IPCE.

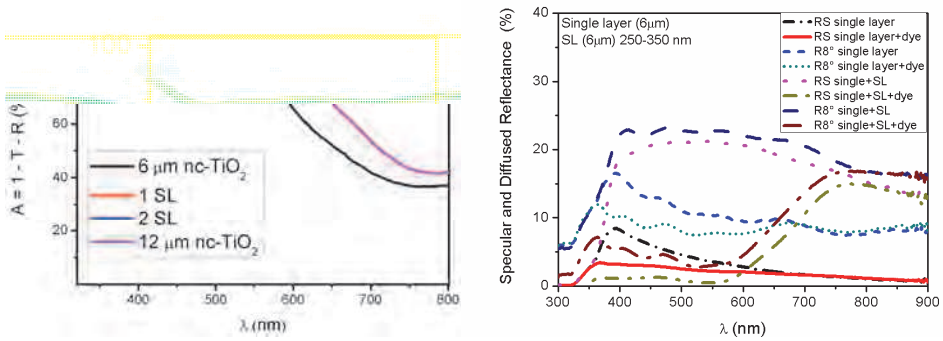

Fig. 19. (Left) Absorption of nc-TiO_2 dyed electrodes and the same covered by one or two diffusive scattering layers. (Right) Diffuse and specular reflectance of the 6 μm titania added by the dye (N719) and not.

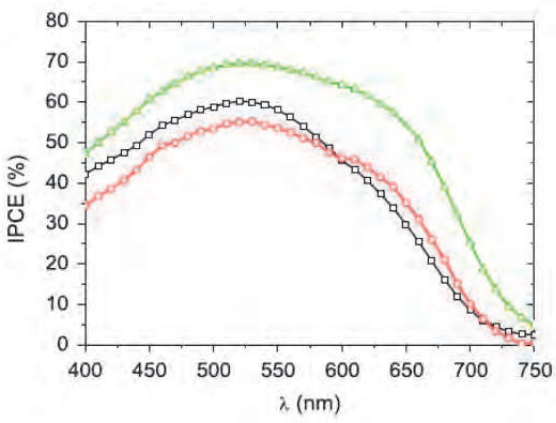

Fig. 20. External Quantum Efficiency of a standard DSC along with two scattering arrangements.

Tipically the IPCE curves have the shape reported in the following figure. In that case thicknesses for both transparent and opaque layers are reported in table 1 (Colonna et al., 2010). The enhancement in the zone over the dye pick has been simply obtained, confirming the idea followed from the above discussion (Usami, 1997).
The electrical values registered are shown in the table. The photocurrent reaches an increment > 45% by using a scattering layer with the same size of the transparent slab, whereas it is quenched by a thicker scattering layer (~ 22 μm).
Finally it is instructive to evaluate the enhancement factor due to the ratio between $IPCE_{SL}$ and $IPCE_{St\text{-}DSC}$. The region of the actual enhancement due to the scattering layer is centered at over 700 nm.

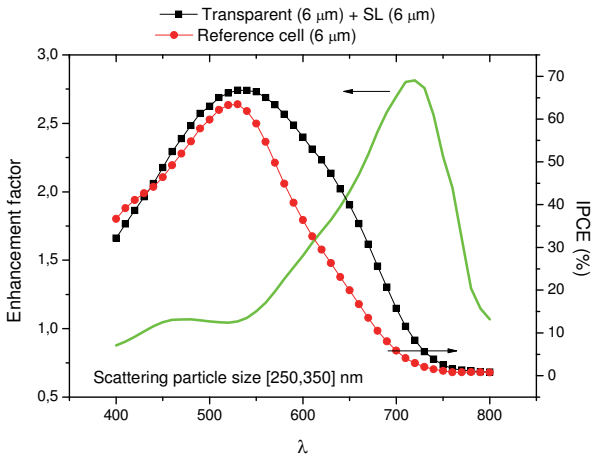

Fig. 21. Single IPCEs for transparent and SL arrangement and enhancement factor due to the SL.

Cell	TiO_2 (μm)	Jsc (mA/cm^2)	Voc (mV)	ff (%)	η (%)
A	12	13.7	710	61	5.93
B	12 + 12	20.2	719	59	8.55
C	12 + 12 + 10	14.4	766	59	6.53

Table 1. Arrangement of photoelectrodes and electric performances of standard DSC (st-DSC) along with scattering structure integrated.

In conclusion the use of larger titania particles for light scattering within the dye sensitized solar cell has been investigated in terms of enhancement in the red region of the spectrum. It has been found that for particular arrangements the photocurrent improvement can reach unprecedented results (Colonna et al., 2010).

4.3 Photonic crystals

One Dimension Photonic Crystals (1DPC) within the DSC assembly represent probably the most important field for future development of the field for several reasons soon described. Up until 2008 it was known from some authors that the integration with inverse opals

(3DPC) could be possible but mechanisms arising in that dye solar cell is different from the one described in the rest of the section since it is coherent scattering effect (Nishimura et al., 2003; Halaoui et al., 2005; Lee et al., 2008; Mihi & Miguez, 2005; Mihi et al., 2006, 2008). The combination of one dimension photonic crystal (1DPCs) layers made by using colloidal solution of SiO_2 and TiO_2 in the dye solar cell technology has been introduced by *S. Colodrero* and *H. Miguez* at CSIC in 2008 as a new powerful tool for DSC technology (Colodrero et al., 2008). They demonstrated the physical properties of the photonic crystal stack in terms of modes of the light once has passed through the multilayer assembly (Colodrero et al., 2009a; Colodrero et al., 2009b; Lozano et al., 2010). The materials integrated on the nc-TiO_2 is composed by alternating SiO_2 (n_{SiO2} ~ 1,5) and TiO_2 (n_{TiO2} ~ 2,5). The periodic arrangement of layers creates patterns of waves interfering in a range of wavelength depending on the thicknesses of each layer when the light is reflected. This imply that the DSC-PCs based can generate a gain with respect to a standard DSC because both the incoming polychromatic light stimulates transitions (standard process) and the reflected PC's band is sent back into the cell. Moreover the arrangement of silica-titania bi-layers creates a periodic refractive index responsible of the photonic band, causing the structural color of the photoanode (Calvo et al., 2008). The Bragg's law implies that the reflected wavelength due to an *optical thickness* of $n_1d_1 + n_2d_2$ is:

$$\lambda_B = 2(n_1 d_1 + n_2 d_2) \tag{4}$$

where the factor 2 refers to the double verse (in and out) of the optical path. The emission photonic band can be calculated by considering the Distributed Bragg Reflector (DBR) used for waveguides. In this case the *photonic stop band* is given by the formula:

$$\Delta\lambda_B = \frac{4\lambda_B}{\pi} asin\left[\frac{n_2 - n_1}{n_1 + n_2}\right] \tag{5}$$

where λ_B derives from the (1). This band represents the optical range of reflected wavelength on the alloy and for the materials used in this study for example with a λ_B = 650 nm, the $\Delta\lambda_B$ is ca. 200 nm (see figure 2). The intensity of the reflectance is given by:

$$R = \left[\frac{(n_0)(n_2)^{2N} - (n_S)(n_1)^{2N}}{(n_0)(n_2)^{2N} + (n_S)(n_1)^{2N}}\right]^2 \tag{6}$$

where n_0, is the refractive indexes of the entering medium, n_1, n_2 the indexes of the alternating materials and finally n_s the index of the exit material. N is the number of the bi-layers creating the structure.

The PC can be created with a simple reliable procedure (Colodrero et al., 2008) giving the possibility to tailor the optical thickness by varying the operative settings of deposition. It consists in the growth of layers by spin coating technique. The final result is the creation of an stack of porous layers. Due to the porosity itself the electrolyte can infiltrate in the pores where it modifies the dielectric constant, hence causing the variation of refractive index of the layer stack and the reflectance Bragg's peak is consequently red shifted according to the Eq. (4). Therefore the reflectance of the complete DSC device will present reflection at wavelengths corresponding to the previous reported in figure plus a shift to the red because of refractive index variation. The reflection will enhance electrical and optical characteristics

of the standard cell by conferring selective photocurrent enhancement. Indeed the IPCE shows well defined improvement zones corresponding to the reflected range of light.

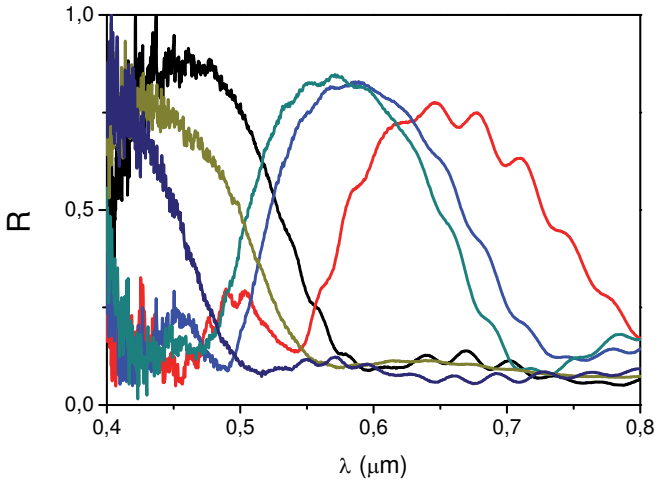

Fig. 22. Reflectance on nc-TiO_2 PEs containing SiO_2/TiO_2 bi-layers measured by FTIR.

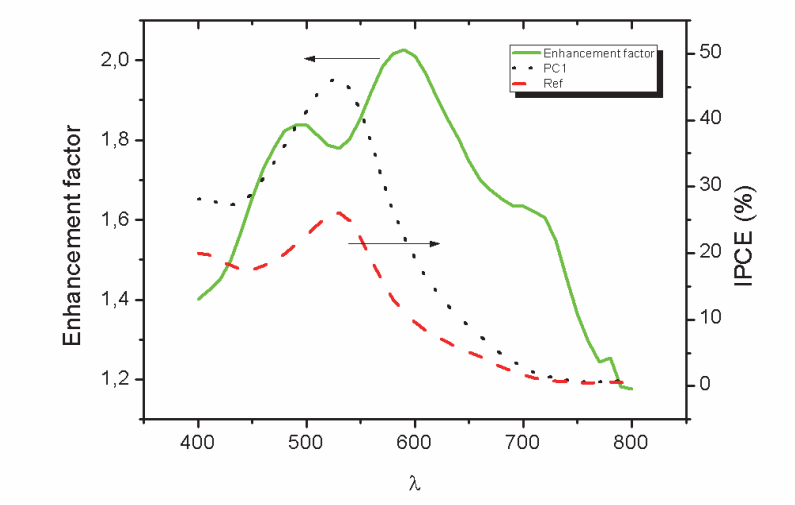

Fig. 23. IPCE enhancement factor calculated by the ratio between the PC integrated and the standard DSC.

The last point is of importance in this development because not only the cell will have high performances, but also a structural coloration will arise independently of the dye color. Finally the important consideration is that the 1DPC-DSC keeps the transparency, meaning that such DSC branch can be further explored for BIPV applications (Colonna et al., 2011b).

4.4 Angular refractive path

Recently (Colonna et al., 2010; Dominici et al., 2010) a strong enhancement of short circuit photocurrent I_{SC} by varying the angle of incidence of a monochromatic laser beam was shown for DSCs. A light path lengthening is active, supposedly, due to the typical features of the absorbing (titania) layer in the semitransparent DSC. I.e., its (relatively) low refractive index n and absorption coefficient a which offer margin improvement for an Angular Refractive Path (ARP) factor to increase the LHE. Indeed, an external oblique incidence θ_a of light corresponds to an oblique angle of propagation θ_{eff} inside the sensitized titania too. The lower the effective index n_{eff} the larger the internal angle θ_{eff}. When $a \cdot h$ is low, an inclination of the propagation line inside the active layer allows to lengthen the path and further absorb light beyond the inherent limit of the native thickness h. Evidence of the ARP factor depends both on the thickness of the cell and the wavelength, plus the eventual use of a coupling prism. The prism allows indeed to reach larger angles of propagation. According to theory, the ARP is shown to be more effective for thinner cells and at wavelengths where the dye molecules absorb less, while the use of the prism enhances it further. The ARP may also explain why DSCs under diffuse illumination work better than other PV technologies, giving hints for new concepts in design of more efficient DSCs.

In order to present evidence of such effect, we initially propose three simple configurations in Fig. 24. The same cell is firstly illuminated in an EQE (i.e., IPCE) setup at θ=00° (normal incidence) retrieving the quantum efficiency spectrum. Then the DSC is rotated and illuminated at a θ=45° angle of incidence. Hence, for the same angle in air (between the light beam and the normal to the cell) a coupling prism is used (half cube, BK7 glass prism). In this last case a matching index oil (n=1.66) is used between the prism (n=1.515) and the glass substrate (n=1.59).

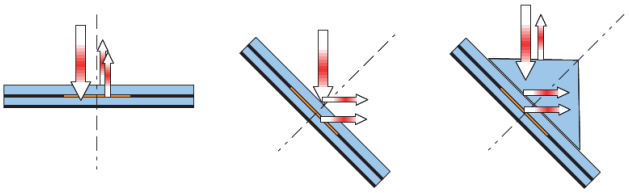

Fig. 24. Three simple configurations to test the refractive angular path. They correspond to normal incidence (θ=00°) without prism, oblique incidence (θ=45°) without prism and oblique incidence (θ=45°) with prism. To keep the light spot always wholly inside the active area means to have constant impinging power. The external reflections are represented together with reflection from the active layer.

The spectra registered in the wavelength range 400-650nm appear in Fig. 25, from bottom to top following the order of their presentation. There is a certain enhancement deriving from the use of an oblique incidence, further pushed up by the use of the prism. Such enhancement can be represented by normalizing the last two curves to the first one. It presents two main features. Firstly, where the EQE (hence, absorption) is high the enhancement has got a local minimum and vice-versa. This feature is expected as introduced on the basis of the ARP theory, discussed more in detail in the following. Secondly, there is a certain monotonic increase of the enhancement with wavelength. This may derive from a λ dispersion of the refractive index of the porous titania.

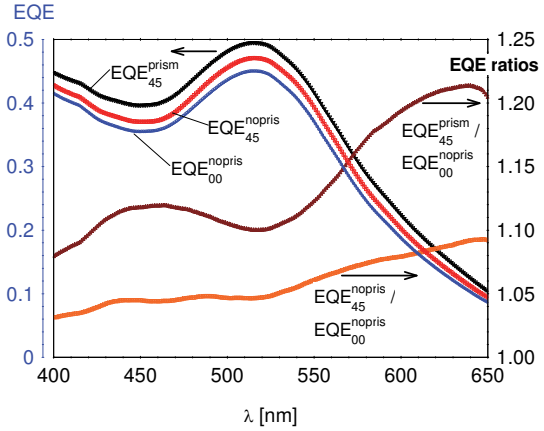

Fig. 25. Measured EQE for three simple configurations on a thin (3μm) DSC. The three configurations correspond to normal incidence (θ=00°) without prism, oblique incidence (θ=45°) without prism and oblique incidence (θ=45°) with prism. The light spot is always wholly inside the active area (impinging power is constant). The enhancement ratios are retrieved normalizing the last two curves to the first one.

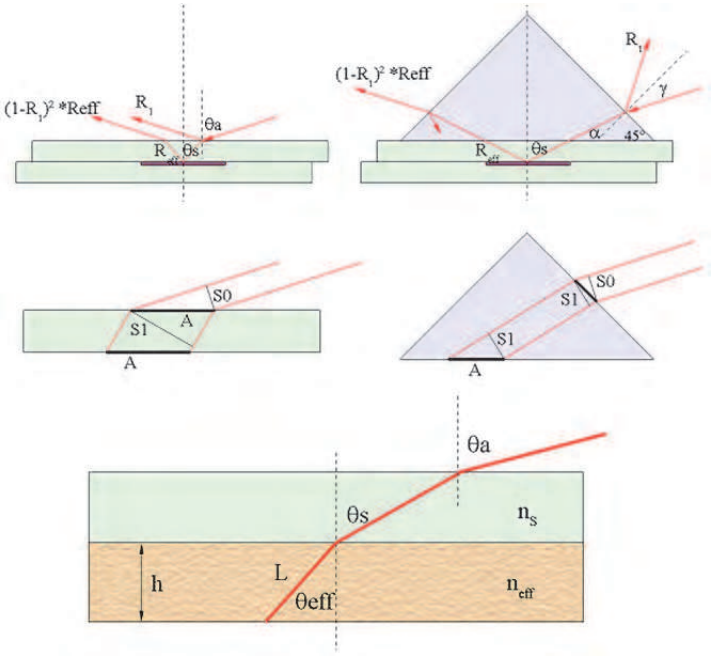

Fig. 26. Mechanism of the three main angular factors in the case of bare device and prism coupling. The considered effects are external reflectivity, projection of the active area and angular refractive path.

Now, the refractive term which we call ARP is not the only acting. Usually angular effects are known as detrimental on the output of photovoltaic devices. This is mainly due to a geometrical factor. When the cell is rotated in a wider light beam, the angular reduction of cross section seen by the cell reduces the collected power according to the *cosine law* (Balenzategui & Chenlo, 2005). Under a sun-simulator, such an effect does not allow to evaluate the other three angular factors we are interested in, since these are important at large angles but are screened by the convolution with the *cosine* term. With the laser, taking care that the spot size of the illuminating beam is always fully contained inside the active area, the impinging power is constant. Hence, the photocurrent measured for each incidence angle is directly proportional to the conversion efficiency and there is no need to take into account the *cosine law*. Instead, we will discuss in the following three other angular factors that are still acting on the photocurrent. These are the external air glass reflectance, the variation of the light intensity and the term of refraction ARP. A schematic of their action mechanism is drawn in the Fig. 26, for without and with coupling prism. The same external angle in air θ_a (considered between the light ray and the normal to the cell substrate) converts in two different angles of propagation inside the substrate θ_s for the bare DSC and with prism. Respectively: $\theta_s=asin(sin\theta_a/n_s)$; $\theta_s=45°-a=45°-asin(sin\gamma/n_s)= 45°-asin[sin(45°-\theta_a)/n_s]$. For simplicity we have used Snell law considering the same refractive index for the prism and the substrate n_s. At the same time, the reflection at their interface may be neglected. The first row of Fig. 26 represent the relevant angles and reflectance. What we consider here is the external air glass reflectance R_1 (in the figure) which varies with the incidence angle. The other one R_{eff} is the reflectance from the active layer (more precisely, multilayer stack). This can be used in attenuated total reflection (ATR) or different setups to study the internal layers but is not of interest here. In the following the external reflectance will be considered by using instead the term of transmittance $T(\theta)=1-R_1(\theta)$. The second row of the Fig. 26 represents the projection area A of the beam over the active area, respect to its external cross section S_0. The projection area affects, together with the transmittance, the light intensity over the titania $I(\theta) \propto T(\theta)/A(\theta)$. Finally, the last row represents the light path L inside the active layer which may be expressed using Snell law again, $L=h/cos\theta_{eff}=h/cos[asin(n_s sin\theta_s/n_{eff})]$. We are indicating the refractive index of the titania layer as an effective index n_{eff} since the nanoporous nature of the titania. It is anchored with dye molecules and its porosity filled with the electrolyte. Hence, according to a Bruggemann effective medium approximation, n_{eff} should be somewhat in between the index of a bulk titania (in anatase phase) and the electrolyte one (mainly due to its solvent).

To represent such angular factors for both bare DSCs and DSC plus prism, we prefer using the internal angle in glass, θ_s. The transmittance $T(\theta)$ term is well known by the Fresnel law which can be applied for both bare DSC and prism configurations. For the bare cell, T appears symmetrical when representing it versus both positive and negative angles of incidence ($-90° \leq \theta_a \leq +90° \Rightarrow -40° < \theta_s < +40°$). The same doesn't hold for the prism and the same full θ_a range converts in an asymmetrical different θ_s range ($+05° < \theta_s < +85°$, when considering a single prism side as the entrance one). In such case, the T factor is a limiting one only for very larger positive angles. In the case of using an adequate emi-cylindrical prism (instead that the half cube one) T would be constant across a full range of θ_s. It should be noted that experimentally, the two ranges cannot be fully explored. At grazing angle the cross section of the substrate or the prism side becomes too small. The variation of the projection area has been represented as S_0/A, retrieved by means of geometrical considerations from the previous Fig. 26 and Snell law once more. In the case of the bare cell such factor follows a

cosine law. Finally, we plot the angular refractive path as $L=h/\cos\theta_{eff}=h/\cos[\text{asin}(n_s \sin\theta_s/n_{eff})]$ for different indexes of the titania layer. The lower the n_{eff} the larger the inclination of the rays, hence the lengthening of the path. The ARP factor depends on θ_{eff} and appears the same for the two configurations, when representing it towards the internal angle θ_s.

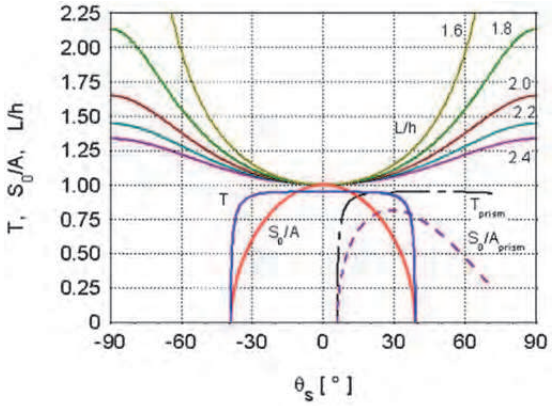

Fig. 27. Computed analytical forms of the three different angular factors that affect I_{SC}. Normalized projection section S_0/A of the beam over the titania (bare cell, bottom central, and with prism, bottom right). Transmitted light power T at the external air/glass interface without (middle central) and with prism (middle right), for the case of unpolarized light. Normalized light path L/h for five different effective indexes of the titania/electrolyte phase (top curves, from bottom to top n_{eff} = 2.4, 2.2, 2.0, 1.8 and 1.6).

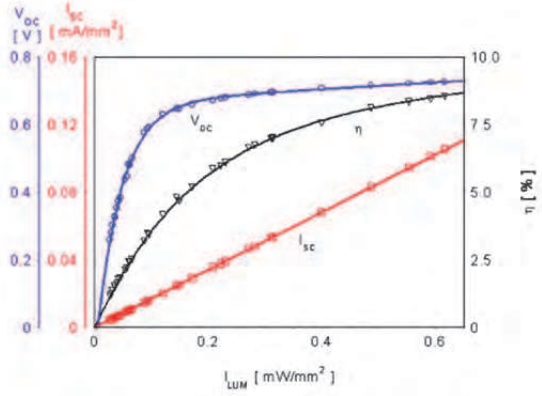

Fig. 28. Main parameters of a DSC measured versus the light intensity at λ=545nm and normal incidence. The I_{SC} could be fitted to a linear curve, while the V_{OC} and the power efficiency η to an exponential plus a linear. The light spot from a lamp was about 8mm² .

In the Fig. 27 the computed variation of the three factor are represented. Using a simple approximation of a Lambert Beer exponential absorption in the sensitized titania, we may write the quantum efficiency as:

$$EQE = LHE \cdot IQE = T(\theta_s) \cdot [1 - e^{-\alpha L(\theta_s)}] \cdot \eta_{inj}\eta_{col} \quad (7)$$

The effect of the second mechanism, the projection area and its influence on the intensity, may be supposed to potentially affect the internal quantum efficiency IQE via one or both of its subterms, the injection η_{inj} and collection η_{col} efficiencies (Trupke et al., 2000). Since the T factor is well known, and we are mainly interested in the refractive path, the effect of the intensity yet unknown needs to be quantified or cleared out in some other way. In the Fig. 28 we report measurements of the main parameters of a standard DSC (thick, h=12μm) towards the intensity I_{LUM} of a monochromatic beam (λ=545nm), at normal incidence (θ_s=0°). The short circuit current I_{SC} keeps linear in the full used range. Hence, in such range there is no apparent dependence of the EQE on the intensity. The following angular measurements were executed with a light intensity which remains inside the I_{LUM} range of Fig. 28.
The Fig. 29 presents angular measurements on thick and thin cells at a wavelength (λ=633nm) where EQE is quite low, about one third of the maximum. The two central curves are the measurements on a standard DSC (thick, h=12μm). The lowest of the two (M-shaped) represents the bare EQE while the upper one (U-shaped) is the EQE normalized to the transmittance T (top solid line, blue on line). As it can be observed the resulting normalized EQE is monotonically increasing with the module of the angle θ. It could be fitted by using the refractive term $1\text{-}e^{-ah/\cos[\arcsin(n_s \sin\theta_s / n_{eff})]}$ retrieving an effective index of n_{eff} = 2.21.

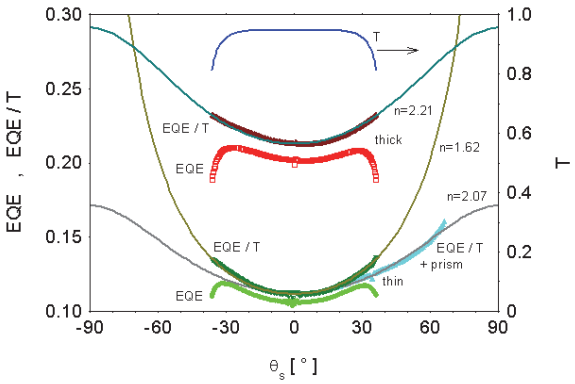

Fig. 29. EQE measured on thick and thin DSCs at λ=633nm. All normalized curves could be fitted to the angular path (Lambert-Beer as a function of the angle). The retrieved effective indexes depend on the specific cell and for a given cell also upon using or not the prism. This may be due to different TiO_2 porosities and thicknesses and to single cell disuniformity.

Experimentally, the symmetry of the curves indicate a proper alignment of the light beam with respect to the axis of rotation. The two bottom central curves represent similar measurements on a thin (h=3μm) cell. In this case, a larger angular enhancement could be seen, considered both in absolute and in percentage values. This is expected since the lower h. The fit with the refractive term is rather good, but the retrieved n_{eff} = 1.62 is much lower than the previous one on the thick cell. This could be ascribed to real differences in the titania layer porosity, but the difference appears to be too large. Another physical effect may be taken into consideration. Increasing the angle, and so the path lengthening, means to effectively absorb photons and generate charges closer to the photoelectrode. So the

electrolyte ions should pass through a longer percolation path across the nanoporous titania. This supposedly influences the collection efficiency η_{col} in a different way between thick and thin cells. An outlook of this work is to investigate such potential effect with electrochemical impedance spectroscopy (EIS) measurements at different angles of incidence.
The bottom curve on the right is the normalized EQE when using the coupling prism on the thin cell. Also now we fitted (somewhat less well at large angles) with the refractive path, but the refractive index is still different (n_{eff} = 2.07) and this time on the same cell. Such aspect is not good and will require further investigations in the future, to reach a good agreement between measurements on the bare cell and the prism case. Experimentally, when excluding the intensity factor, a further issue could be still influencing. Indeed, if spatial disuniformity of the layer is present (hence, of EQE across the active area), the enlargement of the beam projection with the angle could affect the angular trend by sampling regions with different EQE. This could partially explain the observed differences and indicate the importance of having DSCs with a very uniform titania layer for the angular measurements. Another outlook for future implementation is the execution of measurements with also an emi-cylindrical prism and the correlation of the results obtained with all the three coupling elements (bare cell, half-cube prism, emi-cylindrical prism).

5. Conclusions

The technology of the dye solar cells offers nowadays a quite assessed typical configuration. Yet, different strategies are currently under study for increasing the stability and lifetime, but also for the improvement of the energy conversion efficiency. Among such techniques, acting on the main components of the DSCs remains almost a must issue. Traditionally, modifying the titania properties, looking for different fabrications or semiconductors, together with the research of new dyes and electrolytes, still seem a very wide action field, too wide to make sure previsions but surely promising in the actual energetic panorama. Besides, approaches derived from nano photonic and plasmonic technology are being integrated in the dye solar cells with more complex schemes to further improve efficiency in a wide sense of photon management. In such a context, the present work investigated the use of scattering layers, double dye co-sensitization, photonic crystals and also angular refractive path. Till now, the use of diffusive scattering layers led to the best performances. Typical size of the used opaque particles (150 to 400 nanometers) causes along all the wavelengths a reflectance of the non absorbed light back into the cell. Quantitatively the effect caused the improvement of a relative 47% in photocurrent and over 40% in efficiency. The co-sensitization technique was approached by using the conventional Red Dye together with the SDA1570 typically used for dye laser systems. The co-sensitization procedure was showed to be effective, putting into evidence non-linear effects by synergic mechanisms. The performance of co-sensitized cells outperform the sum of those with the single dyes. The immersion of the partially N719-sensitized photoanode in a SDA solution induces the saturation of the remaining free TiO_2 surface and at the same time a partial displacement of the already attached N719 molecules, organizing the two molecules in such a way which limits the energy losses due to the excitonic interactions between homologue molecules. Despite the lower efficiency (~20%) of the co-sensitized DSCs with respect to standard ones, transparency is gained (doubled), confirming as an effective strategy for BIPV applications. The integration of photonic crystals into the DSC for structural coloration represents one of the most engaging results. In fact, despite the color created by the silica/titania multilayer grown onto the nanocrystalline TiO_2 together with the color conferred by the dye itself, the cell is able to enhance the photocurrent and efficiency because of interferential reflections.

Variously colored DSCs were fabricated with the proper designs of the photonic crystals. The PCs schemes led to ca. 60% enhancement in efficiency and ca. 50% in *Jsc*, on thin DSCs, with 3 micrometers thick nc-TiO_2 titania. Also in this case the devices are quite transparent, conferring other important properties / instruments to DSC, i.e. for the building integration. The differences between SLs and PCs arrangements have to be ascribed to their basic issues. Photonic Crystals allow selective reflections based on their structural order, while SLs rely on a random configuration. Hence, PCs effect results in well defined enhancements corresponding to the reflected bands, whereas the typically used SLs lead to an increased absorption at the longer wavelengths with a tailoring at the shorter ones. Finally, the PCs are capable to confer a color independent from the dye color and mostly important keeping a good DSCs transparency; the SLs instead are affected by losing DSCs transparency at all. One main contribution of this work has been to realize and discuss state-of-the-art implementations of all these techniques, which actually are largely studied in the literature. Besides them, also an apparently minor feature was investigated responding to a very basic concept of photon management. The application of an angular setup to illuminate DSCs, allowed to quantify the response of the cells to oblique incidence of light. Apart from the power loss due to the reduction of cross section according to the cosine law, the IPCE rises. The bare cells present a maximum in IPCE at an angle of incidence in between 50° and 60°. This happens although the reflectance of the external air/glass interface grows with angle. Such a feature is ascribed to a photon path lengthening, i.e., an angular refractive path. Upon using a coupling prism two main advantages are obtained. The cut-off in the external transmittance can be overcome and at the same time larger internal angles can be achieved. A simplified yet robust model, based on Fresnel reflectance, Snell law of refraction and Lambert-Beer absorption is able to fit the angular dependencies of the quantum efficiency. The model depends on the effective refractive index of the mesoporous titania layer, which can be set as a fit parameter together with the optical absorbance. Hence, the angular IPCE allows also an investigation of the internal active layer, even though simplified at this stage. The enhancement is active due to the typical features of the thin absorbing titania layer, i.e., its refractive index and absorption coefficient, which offer margin improvements for a ray propagating obliquely to be more absorbed. Hence, it depends on the wavelength, thickness and porosity of the titania layer, but also, for example, on the electrolyte refractive index too. From a photon management point of view, the angular effect has in common with the SLs and PCs to be more effective on thin DSCs and at wavelength where they absorbs less. Unfortunately, its disadvantage is to suffer from the reduction of cross section and power. Nevertheless, it can still give suggestions on structuring DSCs working at normal incidence, and, it cannot be excluded also its potential use in proper new designs of thin films DSCs.

6. References

Abbotto, A.; Barolo, C.; Bellotto, L.; De Angelis, F.; Graetzel, M.; Manfredi, N.; Marinzi, C.; Fantacci, S.; Yum, J.-H. & Nazeeruddin, Md. K. (2008). Electron-rich heteroaromatic conjugated bipyridine based ruthenium sensitizer for efficient dye sensitized solar cells. *Chemical Communications* 42, 5318-5320, doi:10.1039/b900208a

Arakawa, H.; Yamaguchi, T.; Takeuchi, A. & Agatsuma, S. (2006). Efficiency Improvement of Dye-Sensitized Solar Cell by Light Confined Effect, *Conference Record of the IEEE 4th WCPEC*, 1, 36-39, ISBN 1-4244-0017-1, Waikoloa, Hawaii, USA, May 7-12, 2006, doi:10.1109/WCPEC.2006.279340

Arakawa, H.; Yamaguchi, T.; Takeuchi, A.; Okada, K.; Ezure, T. & Tanabe, N. (2007). Solar Cells Module. *JP2007012377 (A)*

Balenzategui, J. L. & Chenlo, F. (2005). Measurement and analysis of angular response of bare and encapsulated silicon solar cells. *Solar Energy Materials and Solar Cells* 86, 1, 53-83, doi:10.1016/j.solmat.2004.06.007

Barnes, P. R. F.; Anderson, A. Y.; Koops, S. E.; Durrant, J. R. & O'Regan, B. C. (2008). Electron injection efficiency and diffusion length in dye-sensitized solar cells derived from incident photon conversion efficiency measurements. *Journal of Physical Chemistry C* 113, 1126-1136

Bisquert, J.; Fabregat-Santiago, F.; Mora-Sero, I.; Garcia-Belmonte, G. & Gimenez, S. (2009). Electron Lifetime in Dye-Sensitized Solar Cells: Theory and Interpretation of Measurements. *Journal of Physical Chemistry C* 113, 40, 17278–17290, doi:10.1021/jp9037649

Buscaino, R.; Baiocchi, C.; Barolo, C.; Medana, C.; Graetzel, M., Nazeeruddin, Md. K. & Viscardi, G. (2007). A mass spectrometric analysis of sensitizer solution used for dye-sensitized solar cell. *Inorganica Chimica Acta* 361, 798–805

Calvo, M. E.; Colodrero, S.; Rojas, T. C.; Anta, J. A.; Ocaña, M. & Míguez, H. (2008). Photoconducting Bragg Mirrors based on TiO2 Nanoparticle Multilayers. *Advanced Functional Materials* 18, 18, 2708-2715, doi:10.1002/adfm.200800039

Catchpole, K. R. & Polman, A. (2008). Plasmonic solar cells. *Optics Express* 16, 26, 21793-21800, doi:10.1364/OE.16.021793

Chappel, S.; Grinis, L.; Ofir, A. & Zaban, A. (2005). Extending the Current Collector into the Nanoporous Matrix of Dye Sensitized Electrodes. *Journal of Physical Chemistry B* 109, 1643-1647, doi:10.1021/jp044949+

Chen, C.-Y.; Wu, S.-J.; Wu, C.-G.; Chen, J.-G.; Ho, K.-C. New ruthenium complexes containing oligoalkylthiophene-substituted 1,10-phenanthroline for nanocrystalline dye-sensitized solar cells. *Advanced Functional Materials* 17, 1, 29–36

Chen, D.; Huang, F.; Cheng, Y.-B. & Caruso, R. A. (2009). Mesoporous Anatase TiO2 Beads with High Surface Areas and Controllable Pore Sizes: A Superior Candidate for High-Performance Dye-Sensitized Solar Cells. *Advanced Materials* 21, 21, 2206–2210

Chen, X. & Mao, S. S. (2007). Titanium Dioxide Nanomaterials: Synthesis, Properties, Modifications, and Applications. *Chemical Reviews* 107, 7, 2891−2959, doi:10.1021/cr0500535

Chen, Y.; Zeng, Z.; Li, C.; Wang, W.; Wang X. & Zhang, B. (2005). Highly efficient co-sensitization of nanocrystalline TiO2 electrodes with plural organic dyes. *New Journal of Chemistry* 29, 773-776, doi:10.1039/b502725j

Cid, J.-J.; Yum, J.-H.; Jang, S.-R.; Nazeeruddin, M. K.; Martinez-Ferrero, E.; Palomares, E.; Ko, J.; Graetzel, M. & Torres, T. (2007). Molecular Cosensitization for Efficient Panchromatic Dye-Sensitized Solar Cells. *Angewandte Chemie International Edition* 46, 44, 8358–8362, doi:10.1002/anie.200703106

Clifford, J. N.; Palomares, E.; Nazeeruddin, M. K.; Thampi, R.; Grätzel, M. & Durrant, J. R. (2004). *Journal of American Chemical Society* 126, 18, 5670-5671, doi:10.1021/ja049705h

Colodrero, S.; Ocaña, M. & Míguez, H. (2008). Nanoparticle-based one-dimensional photonic crystals. *Langmuir* 24, 9, 4430-4434

Colodrero, S.; Mihi, A.; Anta, J. A.; Ocaña, M. & Míguez, H. (2009a). Experimental demonstration of the mechanism of light harvesting enhancement in Photonic-Crystal-Based Dye-Sensitized Solar Cells. *Journal of Physical Chemistry C* 113, 4, 1150-1154

Colodrero, S.; Mihi, A.; Haggman, L.; Ocaña, M.; Boschloo, G.; Hagfeldt, A. & Míguez, H. (2009b). Porous One-Dimensional Photonic Crystals Improve the Power-Conversion Efficiency of Dye-Sensitized Solar Cells. *Advanced Materials* 21, 7, 764-770

Colonna, D.; Dominici, L.; D'Ercole, D.; Brunetti, A.; Michelotti, F.; Brown, T. M.; Reale, A. & Di Carlo, A. (2010). *Superlattice and Microstructures* 47, 197-201

Colonna, D.; Colodrero, S.; Miguez, H.; Di Carlo, A. (2011). Introducing structural color in dye sensitized solar cells by using photonic nanostructures: interplay between conversion efficiency and optical properties. [in print]

Colonna, D.; Capogna, V.; Lembo, A.; Reale, A.; Brown, T. M. & Di Carlo, A. (2011). Efficient co-sensitization of nanocrystalline titania photo-anodes of Dye-Sensitized Solar Cells. [in print]

Dai, S.; Wang, K.; Weng, J.; Sui, Y.; Huang, Y.; Xiao, S.; Chen, S.; Hu, L.; Kong, F.; Pan, X.; Shi, C. & Guo, L. (2005). Design of DSC panel with efficiency more than 6%. *Solar Energy Materials and Solar Cells* 85, 447–455

Di Carlo, A.; Reale, A.; Brown, T. M.; Cecchetti, M.; Giordano, F.; Roma, G.; Liberatore, M.; Mirruzzo, V. & Conte, V. (2008). Smart Materials and Concepts for Photovoltaics: Dye Sensitized Solar Cells, In: *Smart Materials for Energy, Communications and Security*, I.A. Luk'yanchuk & D. Mezzane, (Ed.), 97-126, Springer, ISBN 978-1-4020-8795-0 (Print), 978-1-4020-8796-7 (Online), Dordrecht, The Netherlands, doi:10.1007/978-1-4020-8796-7

Ding, I-K.; Zhu, J.; Cai, W.; Moon, S.-J.; Cai, N.; Wang, P.; Zakeeruddin, S. M.; Graetzel, M.; Brongersma, M. L.; Cui, Y. & McGehee, M. D. (2011). Plasmonic Dye-Sensitized Solar Cells. *Advanced Energy Materials* 1, 52-57

Dominici, L.; Vesce, L.; Colonna, D.; Michelotti, F.; Brown, T. M.; Reale, A. & Di Carlo, A. (2010). Angular and prism coupling refractive enhancement in dye solar cells. *Applied Physics Letters* 96, 103302, doi:10.1063/1.3328097

Ezaki, S.; Gonda, I.; Okuyama, Y.; Takashima, A. & Furusaki, K. (2006). Dye Sensitized Solar Cells. *JP2006294423 (A)*

Ferber, J. & Luther, J. (1998). Computer simulations of light scattering and absorption in dye-sensitized solar cells. *Solar Energy Materials and Solar Cells* 54, 1-4, 265-275

Goldstein, J.; Yakupov, I. & Breen, B. (2010). Development of large area photovoltaic dye cells at 3GSolar. *Solar Energy Materials and Solar Cells* 94, 4, 638-641

Graetzel, M. (2005). Solar energy conversion by dye-sensitized photovoltaic cells. *Inorganic Chemistry* 44, 20, 6841-6851

Gutierrez-Tauste, D.; Zumeta, I.; Vigil, E.; Hernandez-Fenollosa, M. A.; Domenech, X. & Ayllon, J. A. (2005). New low-temperature preparation method of the TiO2 porous photoelectrode for dye-sensitized solar cells using UV irradiation. *Journal of Photochemistry and Photobiology A: Chemistry* 175, 165-171 doi:10.1016/j.jphotochem.2005.04.031

Hagfeldt, A. & Graetzel, M. (1995). Light-Induced Redox Reactions in Nanocrystalline Systems. *Chemical Reviews* 95, 1, 49-68, doi:10.1021/cr00033a003

Hägglund, C.; Zäch, M. & Kasemo, B. (2008). Enhanced charge carrier generation in dye sensitized solar cells by nanoparticle plasmons. *Applied Physics Letters* 92, 1, 013113, doi:10.1063/1.2830817

Halaoui, L. I.; Abrams, N. M. & Mallouk, T. (2005). Increasing the conversion efficiency of dye-sensitized TiO2 photoelectrochemical cells by coupling to photonic crystals. *Journal of Physical Chemistry B*, 109, 13, 6334-6342

Halme, J.; Boschloo, G.; Hagfeldt, A. & Lund, P. (2008). Spectral Characteristics of Light Harvesting, Electron Injection, and Steady-State Charge Collection in Pressed TiO2 Dye Solar Cells. *Journal of Physical Chemistry C* 112, 5623-5637, doi:10.1021/jp711245f

Hinsch, A.; Kroon, J. M.; Kern, R.; Uhlendorf, I.; Holzbock, J.; Meyer, A. & Ferber, J. Long-term stability of dye-sensitised solar cells (2001). *Progress in Photovoltaics: Research and Applications* 9, 6, 425–438, doi:10.1002/pip.397

Hinsch, A.; Behrens, S.; Berginc, M.; Bönnemann, H.; Brandt, H.; Drewitz, A.; Einsele, F.; Faßler, D.; Gerhard, D.; Gores, H.; Haag, R.; Herzig, T.; Himmler, S.; Khelashvili, G.; Koch, D.; Nazmutdinova, G.; Opara-Krasovec, U.; Putyra, P.; Rau, U.; Sastrawan, R.; Schauer, T.; Schreiner, C.; Sensfuss, S.; Siegers, C.; Skupien, K.; Wachter, P.; Walter, J.; Wasserscheid, P.; Würfel, U. & Zistler, M. (2008). Material Development for Dye Solar Modules: Results from an Integrated Approach. *Progress in Photovoltaics: Research and Applications* 16, 6, 489–501

Hore, S.; Nitz, P.; Vetter, C.; Prahl, C.; Niggemann, M. & Kern, R. (2005). Scattering spherical voids in nanocrystalline TiO2 - enhancement of efficiency in dye-sensitized solar cells. *Chemical Communications* 15, 2011-2013, doi:10.1039/B418658N

Hore, S.; Vetter, C.; Kern, R.; Smit, H. & Hinsch, A. (2006). Influence of scattering layers on efficiency of dye-sensitized solar cells. *Solar Energy Materials and Solar Cells* 90, 9, 1176-1188, doi:10.1016/j.solmat.2005.07.002

Ito, S.; Matsui, H.; Okada, K.; Kusano, S.; Kitamura, T.; Wada, Y. & Yanagida, S. (2004). Calibration of solar simulator for evaluation of dye-sensitized solar cells. *Solar Energy Materials and Solar Cells* 82, 3, 421-429, doi:10.1016/j.solmat.2004.01.030

Ito, S.; Nazeeruddin, M.; Liska, P.; Comte, P.; Charvet, R.; Pechy, P.; Jirousek, M.; Kay, A.; Zakeeruddin, S. & Graetzel, M. (2006). Photovoltaic Characterization of Dye-sensitized Solar Cells: Effect of Device Masking on Conversion Efficiency. *Progress in photovoltaics: research and applications* 14, 7, 589-601

Ito, S.; Chen, P.; Comte, P.; Nazeeruddin, M. K.; Liska, P.; Pechy, P. & Graetzel, M. (2007). Fabrication of screen-printing pastes from TiO2 powders for dye-sensitised solar cells. *Progress in photovoltaics: research and applications,* 15, 6, doi:10.1002/pip.768

Kalyanasundaram, K. & Graetzel, M. (1998). Applications of functionalized transition metal complexes in photonic and optoelectronic devices. *Coordination Chemistry Reviews* 177, 1, 347-414

Kay, A. (1995). Dye-stabilised photovoltaic cell module. *DE4416247 (A1)*

Khelashvili, G.; Behrens, S.; Weidenthaler, C.; Vetter, C.; Hinsch, A.; Kern, R.; Skupien, K.; Dinjus, E. & Bonnemann, H. (2006). Catalytic platinum layers for dye solar cells: A comparative study. *Thin Solid Films*, 511–512, 342–348, doi:10.1016/j.tsf.2005.12.059

Kim, C.; Lior, N. & Okuyama, K. (1996). Simple mathematical expressions for spectral extinction and scattering properties of small size-parameter particles, including examples for soot and TiO2. *Journal of Quantitative Spectroscopy and Radiative Transfer* 55, 3, 391-411, doi:10.1016/0022-4073(95)00160-3

Kim, H.; Auyeung, R. C. Y.; Ollinger, M.; Kushto, G. P.; Kafafi, Z. H. & Piqué, A. (2006). Laser-sintered mesoporous TiO2 electrodes for dye-sensitized solar cells. *Applied Physics A: Materials Science & Processing* 83, 1, 73-76, doi:10.1007/s00339-005-3449-0

Kim, S. S.; Nah, Y. C.; Noh, Y. Y.; Jo, J. & Kim, D. Y. (2006). Electrodeposited Pt for cost-efficient and flexible dye-sensitized solar cells. *Electrochimica Acta*, 51, 3814–3819, doi:10.1016/j.electacta.2005.10.047

Koide, N. & Han, L. (2004). Measuring methods of cell performance of dye-sensitized solar cells. *Review Of Scientific Instruments* 75, 9, 2828-2831, doi:10.1063/1.1784556

Koo, H. J.; Park, J.; Yoo, B.; Yoo, K.; Kim, K. & Park, N. G. (2008). Size-dependent scattering efficiency in dye-sensitized solar cell. *Inorganica Chimica Acta* 361, 3, 677-683

Koops, S. E. & Durrant, J. R. (2008). Transient emission studies of electron injection in dye sensitised solar cells. *Inorganica Chimica Acta* 361, 3, 663-670

Kroon, J. M.; Bakker, N. J.; Smit, H. J. P.; Liska, P.; Thampi, K. R.; Wang, P.; Zakeeruddin, S. M.; Grätzel, M.; Hinsch, A.; Hore, S.; Würfel, U.; Sastrawan, R.; Durrant, J. R.; Palomares, E.; Pettersson, H.; Gruszecki, T.; Walter, J.; Skupien, K. & Tulloch, G. E. (2007). Nanocrystalline dye-sensitized solar cells having maximum performance. *Progress in Photovoltaics: Research and Applications* 15, 1, 1-18, doi:10.1002/pip.707

Kuang, D.; Walter, P.; Nuesch, F.; Kim, S.; Ko, J.; Comte, P.; Zakeeruddin, S. M.; Nazeeruddin, M. K. & Graetzel, M. (2007). Co-sensitization of Organic Dyes for Efficient Ionic Liquid Electrolyte-Based Dye-Sensitized Solar Cells. *Langmuir* 23, 10906-10909, doi: 10.1021/la702411n

Lee, S.-H. A.; Abrams, N. M.; Hoertz, P. G.; Barber, G. D.; Halaoui, L. I. & Mallouk, T. E. (2008). Coupling of Titania Inverse Opals to Nanocrystalline Titania Layers in Dye-Sensitized Solar Cells. *Journal of Physical Chemistry B* 112, 46, 14415–14421

Lindström, H.; Magnusson, E.; Holmberg, A.; Södergren, S.; Lindquist, S.-E. & Hagfeldt, A. (2002). A new method for manufacturing nanostructured electrodes on glass substrates. *Solar Energy Materials and Solar Cells* 73, 91, doi:10.1016/S0927-0248(01)00114-3

Lozano, G.; Colodrero, S.; Caulier, O.; Calvo, M. E. & Miguez, H. (2010). Theoretical Analysis of the Performance of One-Dimensional Photonic Crystal-Based Dye-Sensitized Solar Cells. *Journal of Physical Chemistry C* 114, 8, 3681–3687

Meyer, T.; Martineau, D.; Azam, A. & Meyer, A. (2007). All Screen Printed Dye Solar Cell, *Proceeding of SPIE* 6656, 665608.1-665608.11, ISBN 978-0-8194-6804-8, San Diego, California, USA, August 28-30, 2007

Meyer, T.; Scott, M.; Martineau, D.; Meyer, A. & Cainaud, Y. (2009). Turning the dye solar cell into a product, *3rd International Conference Industrialization of DSC, DSC-IC 09*, Nara, Japan, April 22-24, 2009

Mihi, A. & Miguez, H. (2005). Origin of Light-Harvesting Enhancement in Colloidal-Photonic-Crystal-Based Dye-Sensitized Solar Cells. *Journal of Physical Chemistry B* 109, 15968-15976

Mihi, A.; López-Alcaraz, F. J. & Míguez, H. (2006). Full spectrum enhancement of the light harvesting efficiency of dye sensitized solar cells by including colloidal photonic crystal multilayers. *Applied Physics Letters* 88, 193110

Mihi, A.; Calvo, M.; Anta, J. A. & Miguez, H. (2008). Spectral Response of Opal-Based Dye-Sensitized Solar Cells. *Journal of Physical Chemistry* C 112, 1, 13-17

Mincuzzi, G.; Vesce, L.; Reale, A.; Di Carlo, A. & Brown, T. M. (2009). Efficient sintering of nanocrystalline titanium dioxide films for dye solar cells via raster scanning laser *Applied Physics Letters* 95, 103312, doi:10.1063/1.3222915

Mincuzzi, G.; Vesce, L.; Liberatore, M.; Reale, A.; Di Carlo, A. & Brown, T. M. (2011). Dye Laser Sintered TiO_2 Films for Dye Solar Cells Fabrication: an Electrical, Morphological and Electron Lifetime Investigation. *IEEE Transaction on Electron Devices*, doi:10.1109/TED.2011.2160643 [in print]

Murakami, T. N. & Graetzel, M. (2008). Counter electrodes for DSC: Application of functional materials as catalysts. *Inorganica Chimica Acta* 361, 572–580

Nazeeruddin, M.; Kay, A.; Rodicio, I.; Humphry-Baker, R.; Muller, E.; Liska, P.; Vlachopoulos, N. & Graetzel, M. (1993). Conversion of light to electricity by cis-X2bis(2,2'-bipyridyl-4,4'-dicarboxylate)ruthenium(II) charge-transfer sensitizers (X = Cl-, Br-, I-, CN-, and SCN-) on nanocrystalline titanium dioxide electrodes. *Journal of the American Chemical Society* 115, 14, 6382, doi:10.1021/ja00067a063

Nazeeruddin, M. K.; De Angelis, F.; Fantacci, S.; Selloni, A.; Viscardi, G.; Liska, P.; Ito, S.; Takeru, B. & Graetzel, M. (2005). Combined Experimental and DFT-TDDFT

Computational Study of Photoelectrochemical Cell Ruthenium Sensitizers. *Journal of the American Chemical Society* 127, 16835-16847, doi:10.1021/ja052467l

Nishimura, S.; Abrams, N.; Lewis, B. A.; Halaoui, L. I.; Mallouk, T. E.; Benkstein, K. D.; Van de Lagemaat, J. & Frank, A. J. (2003). Standing wave enhancement of red absorbance and photocurrent in dye-sensitized titanium dioxide photoelectrodes coupled to photonic crystals. *Journal of the American Chemical Society* 125, 20, 6306-6310

Ogura, R. Y.; Nakane, S.; Morooka, M.; Orihashi, M.; Suzuki, Y. & Noda, K. (2009). High-performance dye-sensitized solar cell with a multiple dye system. *Applied Physics Letters* 94, 073308, doi:10.1063/1.3086891

Okada, K. & Tanabe, N. (2006). Dye-Sensitized Solar cell and its manufacturing method. *JP2006236960 (A)*

Ono, T.; Yamaguchi, T. & Arakawa, H. (2009). Study on dye-sensitized solar cell using novel infrared dye. *Solar Energy Materials and Solar Cells* 93, 831–835

O'Regan, B. & Graetzel, M. (1991). A low-cost, high-efficiency solar cell based on dye-sensitized colloidal TiO2 films. *Nature* 353, 737-740, doi:10.1038/353737a0

Pan, H.; Ko, S. H.; Misra, N. & Grigoropoulos, C. P. (2009). Laser annealed composite titanium dioxide electrodes for dye-sensitized solar cells on glass and plastics. *Applied Physics Letters* 94, 071117, doi:10.1063/1.3082095

Pala, R. A.; White, J.; Barnard, E.; Liu, J. & Brongersma, M. L. (2009). Design of Plasmonic Thin-Film Solar Cells with Broadband Absorption Enhancements. *Advanced Materials* 21, 1-6

Pandey, S. S.; Inoue, T.; Fujikawa, N.; Yamaguchi, Y. & Hayase, S. (2010). Substituent effect in direct ring functionalized squaraine dyes on near infra-red sensitization of nanocrystalline TiO2 for molecular photovoltaics. *Journal of Photochemistry and Photobiology A: Chemistry* 214, 2-3, 269-275

Park, N.-G. (2010). Light management in dye-sensitized solar cell. *Korean Journal of Chemical Engineering* 27, 2, 375-384, doi:10.2478/s11814-010-0112-z

Peter, L. M. & Wijayantha, K. G. U. (2000). Electron transport and back reaction in dye sensitised nanocrystalline photovoltaic cells. *Electrochimica Acta* 45, 28, 4543-4551, doi:10.1016/S0013-4686(00)00605-8

Pettersson, H.; Gruszecki, T.; Bernhard, R.; Häggman, L.; Gorlov, M.; Boschloo, G.; Edvinsson, T.; Kloo, L. & Hagfeldt A. (2007). The monolithic muticell: A tool for testing material components in dye-sensitized solar cells, *Progress in Photovoltaics: Research and Applications* 15, 113-121

Pichot, F.; Pitts, J. R. & Greg, B. A. (2000). Low-Temperature Sintering of TiO2 Colloids: Application to Flexible Dye-Sensitized Solar Cells. *Langmuir*, 16, 13, 5626–5630, doi:10.1021/la000095i

Polo, A. S.; Itokazu, M. K. & Murakami Iha, N. Y. (2004). Metal complex sensitizers in dye-sensitized solar cells. *Coordination Chemistry Reviews* 248, 1343-1361 doi:10.1016/j.ccr.2004.04.013

Rühle, S.; Greenwald, S.; Koren, E. & Zaban, A. (2008). Optical Waveguide Enhanced Photovoltaics. *Optics Express* 16, 26, 21801-21806, doi:10.1364/OE.16.021801

Saito, Y.; Kitamura, T.; Wada, Y. & Yanagida, S. (2002). Application of Poly(3,4-ethylendioxythiophene) to Counter Electrode in Dye-Sensitized Solar Cells. *Chemistry Letters* 31, 10, 1060, doi:10.1246/cl.2002.1060

Saito, Y.; Kubo, W.; Kitamura, T.; Wada, Y. & Yanagida, S. (2004). I-/I-3(-) redox reaction behavior on poly(3,4-ethylenedioxythiophene) counter electrode in dye-sensitized solar cells. *Journal of Photochemistry and Photobiology A: Chemistry* 164, 1-3, 153-157, doi:10.1016/j.jphotochem.2003.11.01

Sastrawan, R.; Beier, J.; Belledin, U.; Hemming, S.; Hinsch, A.; Kern, R.; Vetter, C.; Petrat, F. M.; Prodi-Schwab, A.; Lechner, P. & Hoffmann, W. (2006). A glass frit-sealed dye solar cell module with integrated series connections. *Solar Energy Materials and Solar Cells* 90, 11, 1680-1691

Schlichthorl, G.; Park, N. G. & Frank, A. J. (1999). Evaluation of the Charge-Collection Efficiency of Dye-Sensitized Nanocrystalline TiO2 Solar Cells. *Journal of Physical Chemistry B* 103, 5, 782-791, doi:10.1021/jp9831177

Seaman, C. H. (1982). Calibration of solar cells by the reference cell method—The spectral mismatch problem. *Solar Energy* 29, 4, 291-298, doi:10.1016/0038-092X(82)90244-4

Shah, A.; Torres, P.; Tscharner, R.; Wyrsch, N. & Keppner, H. (1999). Photovoltaic Technology: The Case for Thin-Film Solar Cells. *Science* 285, 5428, 692-698

Solaronix S.A., April 2011 prod. spec. retrieved from http://www.solaronix.com/products/

Somani, P. R.; Dionigi, C.; Murgia, M.; Palles, D.; Nozar, P. & Ruani, G. (2005). Solid-state dye PV cells using inverse opal TiO2 films. *Solar Energy Materials and Solar Cells* 87, 513–519

Sommeling, P. M.; Rieffe, H. C.; van Roosmalen, J. A. M.; Schönecker, A.; Kroon, J. M.; Wienke, J. A. & Hinsch, A. (2000). Spectral response and IV-characterization of dye-sensitized nanocrystalline TiO2 solar cells. *Solar Energy Materials and Solar Cells* 62, 4, 399-410, doi:10.1016/S0927-0248(00)00004-0

Sommeling, P. M.; Späth, M.; Smit, H. J. P.; Bakker, N. J. & Kroon, J. M. (2004). Long-term stability testing of dye-sensitized solar cells. *Journal of Photochemistry and Photobiology A: Chemistry* 164, 137–144

Suzuki, K.; Yamaguchi, M.; Kumagai, M. & Yanagida, S. (2003). Application of Carbon Nanotubes to Counter Electrodes of Dye-sensitized Solar Cells. *Chemistry Letters* 32, 1, 28-29

Trupke, T.; Würfe, P. & Uhlendorf, I. (2000). Dependence of the Photocurrent Conversion Efficiency of Dye-Sensitized Solar Cells on the Incident Light Intensity. *Journal of Physical Chemistry B*, 104, 48, 11484–11488, doi:10.1021/jp001392z

Tulloch, G. E. (2004). Light and energy-dye solar cells for the 21st century. *Journal of Photochemistry and Photobiology A: Chemistry* 164, 1-3, 209-219, doi:10.1016/j.jphotochem.2004.01.027

Tulloch, G. E. & Skryabin, I. L. (2006). Photoelectrochemical devices. *KR20060035598 (A)*

Tvingstedt, K.; Persson, N.-K.; Inganäs, O.; Rahachou, A. & Zozoulenko, I. V. (2007). Surface plasmon increase absorption in polymer photovoltaic cells. *Applied Physics Letters* 91, 113514, doi:10.1063/1.2782910

Tvingstedt, K.; Dal Zilio, S.; Inganäs, O. & Tormen, M. (2008). Trapping light with micro lenses in thin film organic photovoltaic cells. *Optics Express* 16, 26, 21608-21615

Uchida, S.; Tomiha, M.; Masaki, N.; Miyazawa, A. & Takizawa, H. (2004). Preparation of TiO2 nanocrystalline electrode for dye-sensitized solar cells by 28 GHz microwave irradiation. *Solar Energy Materials and Solar Cells* 81, 135–139, doi:10.1016/j.solmat.2003.08.020.

Usami, A. (1997). Theoretical study of application of multiple scattering of light to a dye-sensitized nanocrystalline photoelectrichemical cell. *Chemical Physics Letters* 277, 1-3, 105-108, doi:10.1016/S0009-2614(97)00878-6

Van de Lagemaat, J.; Park, N. G. & Frank, A. J. (2000). Comparison of Dye-Sensitized Rutile - and Anatase-Based TiO2 Solar Cells. *Journal of Physical Chemistry B* 104, 2044-2052, doi:10.1021/jp9943651

Vesce, L.; Riccitelli, R.; Soscia, G.; Brown, T. M.; Di Carlo, A. & Reale, A. (2010). Optimization of nanostructured titania photoanodes for dye-sensitized solar cells:

Study and experimentation of $TiCl_4$ treatment. *Journal of Non-Crystalline Solids* 356, 37-40, 1958-1961

Vesce, L.; Riccitelli, R.; Orabona, A.; Brown, T. M.; Di Carlo, A. & Reale, A. (2011). Fabrication of Spacer and Catalytic Layers in Monolithic Dye-sensitized Solar Cells. *Progress in Photovoltaics: Research and Applications* [in print]

Walker, A. B.; Peter, L. M.; Lobato, K. & Cameron, P. J. (2006). Analysis of photovoltage decay transients in dye-sensitized solar cells. *Journal of Physical Chemistry B* 110, 50, 25504-25507

Wang, L.; Fang, X. & Zhang, Z. (2010). Design methods for large scale dye-sensitized solar modules and the progress of stability research. *Renewable and Sustainable Energy Reviews* 14, 3178-3184

Wang, P.; Zakeeruddin, M.; Moser, J. E.; Nazeeruddin, M. K.; Sekiguchi, T. & Graetzel, M. (2003). A stable quasi-solid-state dye sensitized solar cell with an amphiphilic ruthenium sensitizer and polymer gel electrolyte. *Nature Materials* 2, 402-407

Wang, Q.; Moser, J. E. & Graetzel, M. (2005). Electrochemical impedance spectroscopic analysis of dye-sensitized solar cells. *Journal of Physical Chemistry B* 109, 31, 14945-14953

Wang, Z. S.; Yamaguchi, T.; Sugihara, H. & Arakawa, H. (2005). Significant Efficiency Improvement of the Black Dye-Sensitized Solar Cell through Protonation of TiO2 Films. *Langmuir*, 21, 4272-4276, doi:10.1021/la050134w

Watson, T.; Mabbett, I.; Wang, H.; Peter, L. & Worsley, D. (2010). Ultrafast near infrared sintering of TiO2 layers on metal substrates for dye-sensitized solar cells. *Progress in Photovoltaics: Research and Applications*, [in print], doi:10.1002/pip.1041

Wijnhoven, J. E. G. J. & Vos, W. L. (1998). Preparation of Photonic Crystals Made of Air Spheres in Titania. *Science* 281, 5378, 802-804, doi:10.1126/science.281.5378.802

Yao, Q-H.; Meng, F.-S.; Li, F.-Y.; Tian, H. & Huang, C.-H. (2003). Photoelectric conversion properties of four novel carboxylated hemicyanine dyes on TiO2 electrode. *Journal of Materials Chemistry* 13, 5, 1048–1053, doi:10.1039/B300083B

Yip, C.-H.; Chiang, Y.-M. & Wong, C.-C. (2008). Dielectric Band Edge Enhancement of Energy Conversion Efficiency in Photonic Crystal Dye-Sensitized Solar Cell. *Journal of Physical Chemistry C* 112, 23, 8735-8740

Yum, J-H.; Walter, P.; Huber, S.; Rentsch, D.; Geiger, T.; Nuesch, F.; De Angelis, F.; Graetzel, M. & Nazeeruddin, M. K. (2007). Efficient Far Red Sensitization of Nanocrystalline TiO2 Films by an Unsymmetrical Squaraine Dye. *Journal of American Chemical Society* 129, 34, 10320-10321, doi:10.1021/ja0731470

Yum, J.-H.; Moon, S. J.; Humphry-Baker, R.; Walter, P.; Geiger, T.; Nuesch, F.; Graetzel, M. & Nazeeruddin, M. K. (2008). Effect of coadsorbent on the photovoltaic performance of squaraine sensitized nanocrystalline solar cells. *Nanotechnology* 19, 42, 424005, doi:10.1088/0957-4484/19/42/424005

Zhang, D.; Yoshida, T. & Minoura, H. (2003). Low-Temperature Fabrication of Efficient Porous Titania Photoelectrodes by Hydrothermal Crystallization at the Solid/Gas Interface. *Advanced Materials* 15, 10, 814-817, doi:10.1002/adma.200304561

Zhang, Q. F.; Chou, T. P.; Russo, B.; Jenekhe, S. A. & Cao, G. Z. (2008). Polydisperse Aggregates of ZnO Nanocrystallites: A Method for Energy-Conversion-Efficiency Enhancement in Dye-Sensitized Solar Cells. *Advanced Functional Materials* 18, 11, 1654-1660, doi:10.1002/adfm.200701073

Zhou, Y.; Zhang, F.; Tvingstedt, K.; Tian, W. & Inganäs, O. (2008). Multifolded polymer solar cells on flexible substrates. *Applied Physics Letters* 93, 033302, doi:10.1063/1.2957995

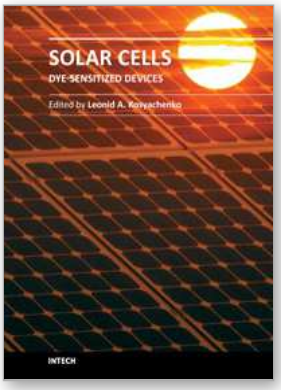

Solar Cells - Dye-Sensitized Devices
Edited by Prof. Leonid A. Kosyachenko

ISBN 978-953-307-735-2
Hard cover, 492 pages
Publisher InTech
Published online 09, November, 2011
Published in print edition November, 2011

The second book of the four-volume edition of "Solar cells" is devoted to dye-sensitized solar cells (DSSCs), which are considered to be extremely promising because they are made of low-cost materials with simple inexpensive manufacturing procedures and can be engineered into flexible sheets. DSSCs are emerged as a truly new class of energy conversion devices, which are representatives of the third generation solar technology. Mechanism of conversion of solar energy into electricity in these devices is quite peculiar. The achieved energy conversion efficiency in DSSCs is low, however, it has improved quickly in the last years. It is believed that DSSCs are still at the start of their development stage and will take a worthy place in the large-scale production for the future.

INTECH
open science | open minds

InTech Europe
University Campus STeP Ri
Slavka Krautzeka 83/A
51000 Rijeka, Croatia
Phone: +385 (51) 770 447
Fax: +385 (51) 686 166
www.intechopen.com

InTech China
Unit 405, Office Block, Hotel Equatorial Shanghai
No.65, Yan An Road (West), Shanghai, 200040, China
中国上海市延安西路65号上海国际贵都大饭店办公楼405单元
Phone: +86-21-62489820
Fax: +86-21-62489821